iScience

CellPress
OPEN ACCESS

Article

Targeting histone methylation to reprogram the transcriptional state that drives survival of drug-tolerant myeloid leukemia persisters

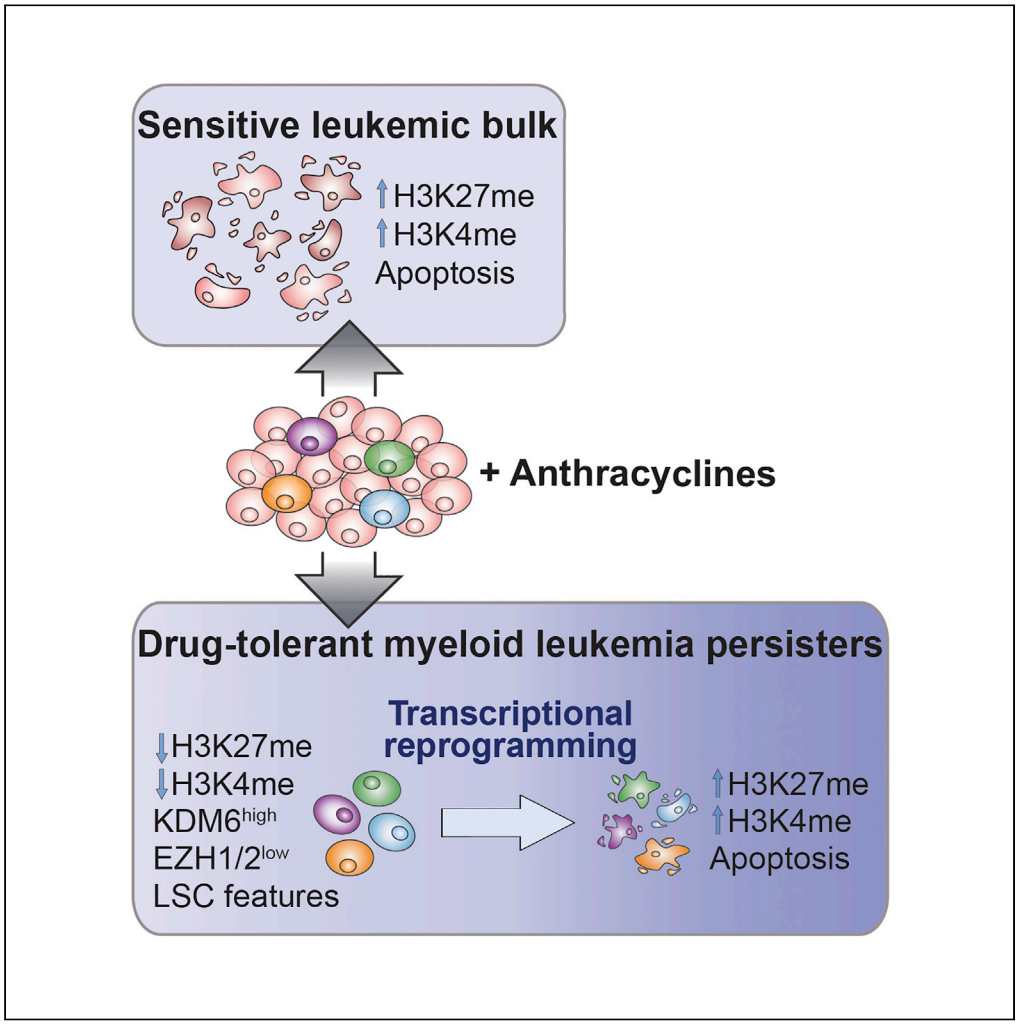

Noortje van Gils, Han J.M.P. Verhagen, Michaël Broux, ..., Gert J. Ossenkoppele, Renee X. Menezes, Linda Smit

li.smit@amsterdamumc.nl

Highlights

Reversible anthracycline-tolerant leukemia cells (ATCs) have low H3K27me3 or H3K4me3

ATCs exhibit stem cell features similar to leukemic stem cells

Reprogramming the transcriptional state by inhibition of KDM6 depletes ATCs

Inhibiting KDM6 adds to doxorubicin treatment and eradicates AML MRD (stem) cells

van Gils et al., iScience *25*, 105013
September 16, 2022
https://doi.org/10.1016/j.isci.2022.105013

iScience

CellPress
OPEN ACCESS

Article

Targeting histone methylation to reprogram the transcriptional state that drives survival of drug-tolerant myeloid leukemia persisters

Noortje van Gils,[1,5] Han J.M.P. Verhagen,[1,5] Michaël Broux,[2,3] Tania Martiáñez,[1] Fedor Denkers,[1] Eline Vermue,[1] Arjo Rutten,[1] Tamás Csikós,[1] Sofie Demeyer,[2,3] Meryem Çil,[1] Marjon Al,[1] Jan Cools,[2,3] Jeroen J.W.M. Janssen,[1] Gert J. Ossenkoppele,[1] Renee X. Menezes,[4] and Linda Smit[1,6,*]

SUMMARY

Although chemotherapy induces complete remission in the majority of acute myeloid leukemia (AML) patients, many face a relapse. This relapse is caused by survival of chemotherapy-resistant leukemia (stem) cells (measurable residual disease; MRD). Here, we demonstrate that the anthracycline doxorubicin epigenetically reprograms leukemia cells by inducing histone 3 lysine 27 (H3K27) and H3K4 tri-methylation. Within a doxorubicin-sensitive leukemia cell population, we identified a subpopulation of reversible anthracycline-tolerant cells (ATCs) with leukemic stem cell (LSC) features lacking doxorubicin-induced H3K27me3 or H3K4me3 upregulation. These ATCs have a distinct transcriptional landscape than the leukemia bulk and could be eradicated by KDM6 inhibition. In primary AML, reprogramming the transcriptional state by targeting KDM6 reduced MRD load and survival of LSCs residing within MRD, and enhanced chemotherapy response *in vivo*. Our results reveal plasticity of anthracycline resistance in AML cells and highlight the potential of transcriptional reprogramming by epigenetic-based therapeutics to target chemotherapy-resistant AML cells.

INTRODUCTION

The majority of AML patients achieve an initial deep response (complete remission) with induction chemotherapy, consisting of cytarabine and an anthracycline (Löwenberg, 2008). However, the five-year survival rate of AML patients is poor, ranging from 35–40% in adults below 60 years to as low as 5–15% in older patients. (Burnett et al., 2011; Löwenberg et al., 1999, 2009). These low cure rates are mainly because of chemotherapy resistance driven by intra-leukemic heterogeneity and plasticity. Often a small subpopulation of leukemia cells survives chemotherapy treatment, so-called measurable residual disease (MRD), and provides the origin of disease recurrence (Terwijn et al., 2013). Leukemia cells initiating relapse residing within MRD are thought to have stem cell features and are therefore named "leukemic stem cells" (LSCs) (Bonnet and Dick, 1997; Ishikawa et al., 2007). The clinical importance of these LSCs has been demonstrated by studies showing an association between treatment outcome and LSC frequency (van Rhenen et al., 2005; Terwijn et al., 2014), and between outcome and expression of LSC-associated genes (Eppert et al., 2011; Ng et al., 2016). Yet, recent studies in mice and patients showed that AML cells that survived cytarabine treatment were not enriched for LSCs (Boyd et al., 2018; Farge et al., 2017).

AML persisters may have pre-existed in the AML bulk population at diagnosis but may also be induced by the therapy. Chemotherapy may induce resistance in cells predisposed to undergo a transcriptional transition that is associated with reduced therapy sensitivity, and may also induce changes in the frequency and phenotype of LSCs (Boyd et al., 2018; Ho et al., 2016), highlighting the need to unravel the transcriptional state of therapy-resistant AML (stem) cells and their associated vulnerabilities after initial treatment.

In parallel to genetic heterogeneity, there is strong evidence that non-genetic factors contribute to intra-leukemic variation in the response to chemotherapy (Easwaran et al., 2014; Meacham and Morrison, 2013). Emergence of drug-resistant cells involves intrinsic transcriptional diversity that is established by integrated functions of transcription factors (TFs) and epigenetic modulators (Cohen et al., 2008; Dalerba

[1]Department of Hematology, Amsterdam UMC, location VUmc, Cancer Center Amsterdam, Amsterdam, the Netherlands

[2]KU Leuven Center for Human Genetics, Leuven, Belgium

[3]VIB Center for Cancer Biology, Leuven, Belgium

[4]Department of Epidemiology and Biostatistics, Amsterdam UMC, location VUmc, Amsterdam, the Netherlands

[5]These authors contributed equally

[6]Lead contact

*Correspondence: li.smit@amsterdamumc.nl

https://doi.org/10.1016/j.isci.2022.105013

et al., 2011; Giustacchini et al., 2017). Anthracyclines, a major component of the current AML therapy, are known to trap type II topoisomerases to DNA, leading to double-strand breaks and apoptosis (Pommier et al., 2010). Anthracyclines can also evict histones from loose chromatin, thereby enhancing nucleosome turnover in promoter regions and changing the transcriptome (Pang et al., 2013; Yang et al., 2014). AML cells with a DNMT3A mutation showed impaired nucleosome eviction and chromatin remodeling, leading to reduced sensitivity to anthracyclines (Guryanova et al., 2016), highlighting again the participation of chromatin in responses to chemotherapy. The most common implicated mechanism for development of anthracycline resistance is increased expression of efflux transporters, such as multidrug resistance (MDR)1 (Nooter et al., 1990; Shaffer et al., 2012). However, in contrast to preclinical studies targeting MDR1 (Mahadevan and List, 2004), the majority of clinical trials evaluating MDR inhibitors in AML patients have been disappointing (Cripe et al., 2010; Van Der Holt et al., 2005; Libby and Hromas, 2010). Here, we evaluated whether reprogramming an anthracycline-resistant state of leukemia cells, by targeting chromatin regulators, might result in successful depletion of doxorubicin-persisters.

Several studies showed the presence of cancer cells with distinct epigenetic and transcriptional states and different sensitivities to therapy within a genetically identical tumor cell population (Göllner et al., 2016; Pisco and Huang, 2015; Sharma et al., 2010). For example, a small epigenetically determined reversible drug-tolerant subpopulation of tumor cells can be the source of tyrosine kinase inhibitor (TKI) resistance (Raha et al., 2014; Sharma et al., 2010; Vinogradova et al., 2016). This TKI resistance could be reversed by drug withdrawal and treatment with histone deacetylase or insulin-like growth factor-1 receptor inhibitors, and showed to be associated with a stem cell-like cancer cell phenotype containing high levels of the histone H3 lysine 4 (H3K4) demethylase (KDM)5A (Sharma et al., 2010). Also cisplatin-selected melanoma cells showed to have reduced H3K4me3 levels and high KDM5A (Roesch et al., 2010), underlining involvement of epigenetic modifiers in development and maintenance of drug-resistant cell populations. Several KDMs, including KDM5 and KDM6, have been implicated in both therapy resistance (Dalvi et al., 2017; Hinohara et al., 2018; Liau et al., 2017; Pisco et al., 2013; Sharma et al., 2010) and persistence of cancer stem cells within solid tumors (Taube et al., 2017; Yan et al., 2017).

KDMs, like methyl transferases, influence histone methylation, affecting gene expression. The repressive chromatin marks di- and tri-methylation of H3K27 (H3K27me2,3) are removed via KDM6A and KDM6B, or placed by enhancer of zeste homolog 2 (EZH2), a component of the polycomb repressive complex 2 (PRC2). Loss of EZH2, and as a consequence low H3K27me3, is associated with resistance to multiple drugs in AML (Göllner et al., 2016). KDM6 is enhanced expressed in AML as compared with normal hematopoietic stem cells (HSCs), and is associated with a worse prognosis (Li et al., 2018). Of interest, at AML diagnosis, reduced H3K27me3 can predict a lack of response to induction therapy and is associated with poor survival (Maganti et al., 2018).

Here we sought to non-genetically characterize the therapy-resistant subpopulation of leukemia cells after treatment with anthracyclines, and identified persister cells that could be reprogrammed for cell death by the inhibition of histone H3K27 demethylases.

RESULTS

Identification of an anthracycline-tolerant subpopulation of myeloid leukemia cells

To study intra-leukemia heterogeneity with respect to anthracycline sensitivity, we seeded K562 myeloid leukemia cells in 480 wells, each containing 10.000 cells, and treated the cells with increasing concentrations of doxorubicin (up to 225 ng/mL) (Figure 1A). K562 cells are derived from the pleural effusion of a patient with chronic myeloid leukemia in terminal myeloid blast crisis, which is characterized by accumulation of immature myeloblasts similar to those found in patients with AML. Four wells showed survival of cells after four weeks of treatment with doxorubicin, implicating clonal outgrowth of four doxorubicin-resistant cells. These anthracycline-tolerant persisters were designated ATCs and could be cultured over a long period of time in the presence of 225 ng/mL doxorubicin. Their growth rate was similar to the parental polyclonal cell population (Figure 1B) and the ATCs were resistant to doxorubicin concentrations up to 10 μM (Figure 1C). Moreover, the ATCs were also resistant to daunorubicin (Figure 1D), confirming their anthracycline-resistant phenotypes.

The relative short development time of the ATCs suggests a non-mutational and therefore transient and reversible mechanism of resistance. Indeed, after culturing the ATCs in the absence of doxorubicin for

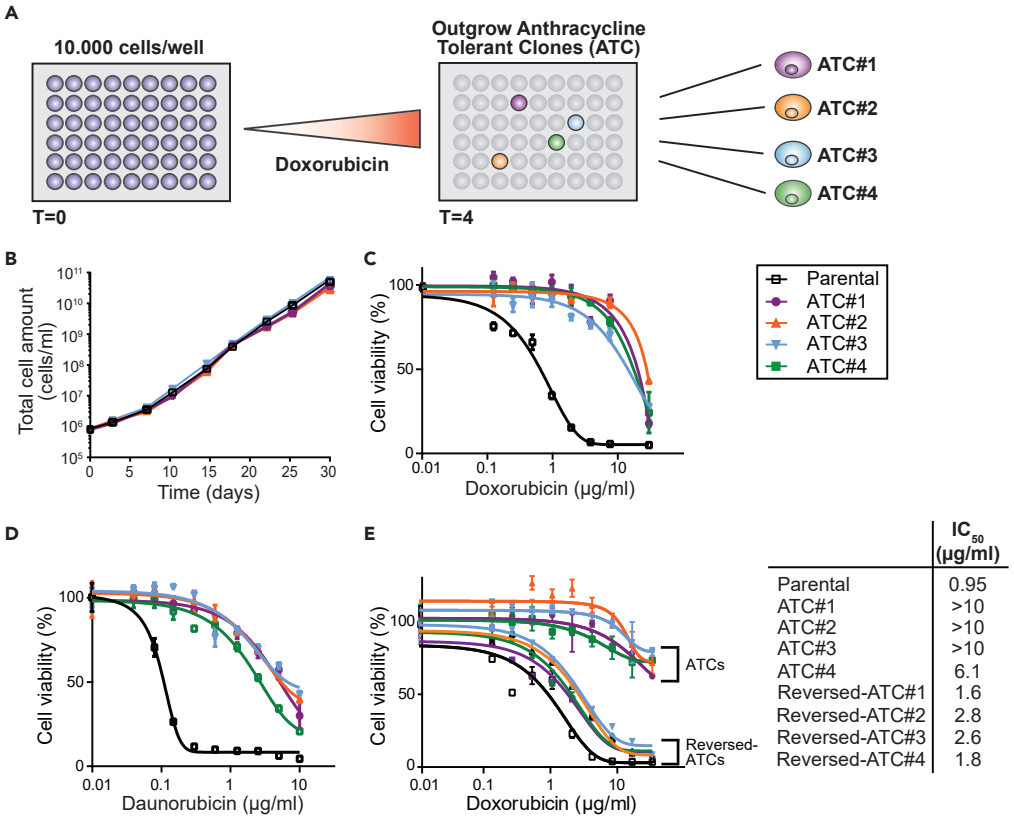

	IC_{50} (µg/ml)
Parental	0.95
ATC#1	>10
ATC#2	>10
ATC#3	>10
ATC#4	6.1
Reversed-ATC#1	1.6
Reversed-ATC#2	2.8
Reversed-ATC#3	2.6
Reversed-ATC#4	1.8

Figure 1. Identification of an anthracycline-tolerant subpopulation of myeloid leukemia cells

(A) Experimental outline to generate anthracycline-tolerant clones (ATCs). K562 cells were seeded in 480 wells with 10,000 cells/well and treated with an increasing concentration of doxorubicin (up to 225 ng/mL). After 4 weeks, cells in 21 wells survived chemotherapy treatment. Subsequently, cells from 4 wells could be maintained in culture in the presence of 225 ng/µL doxorubicin (ATC#1-4).

(B) Growth curve of parental cells and ATCs, seeded at 0.1 × 10^5 cells/mL, passaged 1:5 for 30 days and counted every 3–5 days.

(C–E) ATCs and parental cells were subjected to increasing concentrations of indicated anthracyclines. Cell viability was measured by an MTT assay and depicted as value of treated cells relative to untreated cells. Error bars shows the SEM of a triplicate. Effect of (C) doxorubicin or (D) daunorubicin on cell viability.(E) ATCs were cultured in presence or absence (reversed-ATCs) of doxorubicin for 10 weeks and cell viability was measured after incubation with doxorubicin. IC50: the concentration whereby doxorubicin reduces the cell survival by half.

10 weeks the cells had re-acquired sensitivity for doxorubicin (Figure 1E), suggesting that the anthracycline-resistant phenotype is epigenetically regulated. The withdrawal of doxorubicin resulted in outgrow of drug-sensitive cells, designated as reversed-ATCs, which suggested that anthracyclines can maintain a drug-tolerant state by putting a selective pressure onto leukemia cells, and can change the transcriptional landscape of a few cells within the bulk of a leukemic cell population. The reversed-ATCs obtained sensitivity to doxorubicin with IC50 values between 1.6 and 2.8 µM, which was 1.7– to2.9-fold less sensitive than the original sensitive K562 parental cells.

Doxorubicin induces H3K27 and H3K4 methylation and modulation of gene expression

AML cells can acquire an adaptive state by treatment with chemotherapy (Boyd et al., 2018), which implicates that therapy itself can induce transcriptomic and/or epigenetic changes affecting sensitivity to the treatment. As it has been previously shown that changes in levels of H3K27 and H3K4 methylation in AML cells led to reduced sensitivity to several therapeutics (Göllner et al., 2016; Maganti et al., 2018; Sakamoto et al., 2014; van Dijk et al., 2021), we first investigated whether doxorubicin treatment could affect histone methylation and reprogram the transcriptome. Of interest, after short incubation of parental cells with 225 ng/mL doxorubicin the levels of methylated H3K27 and H3K4 increased (Figure 2A), and a change

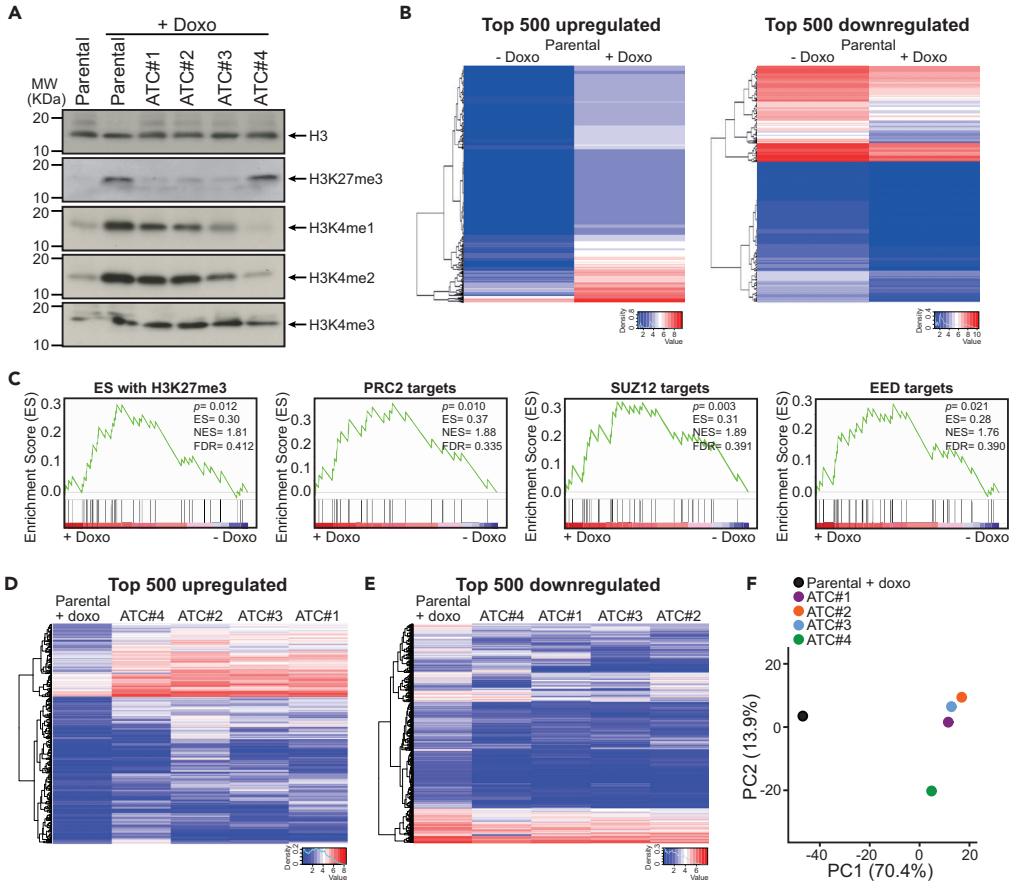

Figure 2. Doxorubicin induces H3K27 and H3K4 methylation and modulation of gene expression

(A) Immunoblot analysis of H3K27 and H3K4 methylation in K562 parental cells stimulated with or without doxorubicin (225 ng/mL) for 48 h and in the ATCs cultured in the presence of doxorubicin (225 ng/mL).

(B–F) K562 parental cells were treated with 225 ng/mL doxorubicin for 48 h. Gene expression profiling (GEP) of these cells and ATCs was performed using RNA-sequencing. Genes were selected based on their log2 fold-change (FC) expression.

(B) Heatmap showing the top 500 genes upregulated and downregulated genes in parental cells after doxorubicin treatment (log2 FC > 2.0 and <-2.0, respectively). Gene expression data is listed in Tables S1 and S2.

(C) GEPs of parental cells treated with doxorubicin were compared to gene sets of H3K27me3 bound genes normally enriched in embryonic stem cells (M10371) and genes known as targets of the PRC2-complex (M8448) and its components SUZ12 (M9898) and EED (M7617) derived from MSigDB (Broad Institute). Enrichment score (ES), normalized enrichment score (NES), false discovery rate (FDR), and p values were calculated using GSEA software (Broad Institute).

(D) Heatmap showing the top 500 genes upregulated (log2 FC > 1.3) and (E) top 500 genes downregulated (log2 FC < −0.8) in the ATCs relative to parental cells incubated with doxorubicin. Genes are listed in Tables S3 and S4.

(F) Principal component (PC) analysis of gene expression from the ATCs and parental cells treated with doxorubicin.

in the transcriptome was observed (Figures 2B, S1A, Table S1 and S2). Transcriptomic changes included several downregulated genes involved in apoptosis and cell survival; for example, BCL2 and STAT5B. Moreover, several of the upregulated genes are associated with Wnt signaling and "stemness", such as SRFP5, Wnt9A, Wnt2B, LRP1, and LRP4 (Figures 2B, S1A, Table S1 and S2). Gene set enrichment analysis (GSEA) revealed that doxorubicin enhanced H3K27me3-bound genes enriched in embryonic stem cells (M10371), and target genes of the epigenetic repression complex PRC2 (M8448) and its components SUZ12 (M9898) and EED (M7617) (Ben-Porath et al., 2008; Lee et al., 2006) (Figure 2C). Pathway analysis using DAVID and protein-protein interaction analysis using String showed upregulation of ABC transporters, extracellular matrix and adhesion molecules, and changes in expression of PI3K-Akt pathway components after doxorubicin treatment (Figures S1B and S1C). Together, these results imply that anthracyclines modify histone methylation and reprogram the transcriptome in leukemia cells, potentially imposing resistance but also novel therapeutic vulnerabilities.

Anthracycline-tolerant leukemia cells have reduced H3K27me or H3K4me, and modulated gene expression profiles

The rapidity and reversibility of development of resistance to doxorubicin in the ATCs supports an epigenetic-mediated tolerance, as has been demonstrated for resistance to targeted therapies (Liau et al., 2017; Sharma et al., 2010). When levels of H3K27 and H3K4 methylation were compared between the ATCs and parental cells, we observed that ATC#1-3 have diminished H3K27me3 levels, whereas ATC#4 has lower H3K4me levels (Figure 2A), suggesting that the resistant cells are incapable of elevating their histone methylation levels after treatment with doxorubicin. To elucidate the transcriptomic state and regulatory circuits involved in the drug-tolerant condition of the persisters we performed RNA sequencing and compared the gene expression profiles (GEPs) of the ATCs with that of the sensitive parental cells shortly treated with doxorubicin (Figures 2D, 2E, Tables S3 and S4). Many genes were modulated in all ATCs, suggesting a general distinct transcriptional state from the anthracycline-sensitive cells. However, there were many mRNAs solely modified in one or more clones, possibly reflecting heterogeneity in mechanisms leading to drug tolerance in the different ATCs (Figure S2A, Tables S3 and S4). The top upregulated gene in all ATCs was MDR1, previously shown to be the most highly upregulated gene in daunorubicin-resistant K562 cells (Williams et al., 2020), and the top downregulated gene ALDH1A1. Pathway analysis using DAVID and protein-protein interaction analysis using String with the up- and downregulated genes that are shared between the 4 ATCs showed differential expression of components of the PI3K-AKT signaling pathway, and enhanced expression of the MAPK, RAS, and Wnt pathway components in the ATCs as compared with the parental cells (Figures S2B and S2C). Principal component analysis revealed again that the ATCs have a distinct transcriptomic state from parental cells shortly treated with doxorubicin (PC1, 70.4% variance; Figure 2F). Interestingly, the transcriptome of ATC#4 is distinct from that of ATC#1–3 (PC2, 13.9% variance; Figure 2F), which is in line with the difference in H3K27 methylation levels between ATC#4 and ATC#1–3 (Figure 2A).

Because H3K27me3 is only diminished in ATC#1–3 (Figure 2A) and ATC#4 has a distinct transcriptional state than the other ATCs (Figure 2F), we decided to focus on ATC#1–3 and the differential H3K27 methylation state in the resistant clones as compared to the sensitive parental cells. First, we evaluated whether regulators of H3K27 methylation are changed by doxorubicin, or differentially expressed in the ATCs as compared to the parental cells. Incubation of the parental cells with doxorubicin resulted in downregulation of several histone demethylases, including the two H3K27 demethylases KDM6A and KDM6B (Figure 3A). Of interest, the ATCs did not show KDM6B downregulation, and ATC#1 even had enhanced KDM6B expression, although the ATCs are cultured in the presence of doxorubicin (Figures 3B andS3A). Validation of KDM6B expression in the ATCs by Q-RT-PCR revealed enhanced expression in ATC#1 and #2, while similar levels as the parental cells in ATC#3 (Figure 3C). To evaluate whether KDM6B activity could be involved in decreased sensitivity to doxorubicin, parental cells were transiently transfected with constructs leading to overexpression of wild-type or catalytic inactive mutant KDM6B (Figure S3B). 4-fold lower sensitivity for doxorubicin was observed in cells overexpressing KDM6B compared to control cells (IC_{50} of 68.1 ng/mL versus 16.4 ng/mL, respectively). This effect is dependent on the demethylase activity of KDM6B since doxorubicin sensitivity was unaffected in cells expressing the catalytic inactive mutant (IC_{50} of 16.0 ng/mL) (Figure 3D).

Next to histone demethylases, H3K27 methylation levels are modulated by components of the PRC2 complex. Therefore, we measured EZH1, EZH2, SUZ12, and EED protein levels in parental cells treated with doxorubicin and in the ATCs, and showed that doxorubicin reduced EZH1, EZH2 and SUZ12. Notably, the ATCs had even lower levels of these proteins than the doxorubicin-treated parental cells (Figure 3E). Together, these results suggest that low H3K27me3 levels in the persisters might be the result of a lack of downregulation of KDM6B and/or reduced EZH1/2 or SUZ12 levels after treatment with doxorubicin.

The distinct transcriptional state of the ATCs might have been present before treatment or acquired as an adaptive response to doxorubicin. To determine which pathways changed in ATC#1–3 as a result of the doxorubicin treatment, we compared genes differentially expressed between the resistant and sensitive cells, with those modulated by doxorubicin. This comparison revealed 48 up- and 6 downregulated genes (Figure 3F and Table S5). Pathway analysis of these 54 genes showed increased expression of cell surface proteins and modulated expression of PI3K-AKT signaling pathway components induced by doxorubicin especially in the ATCs (Figure 3G).

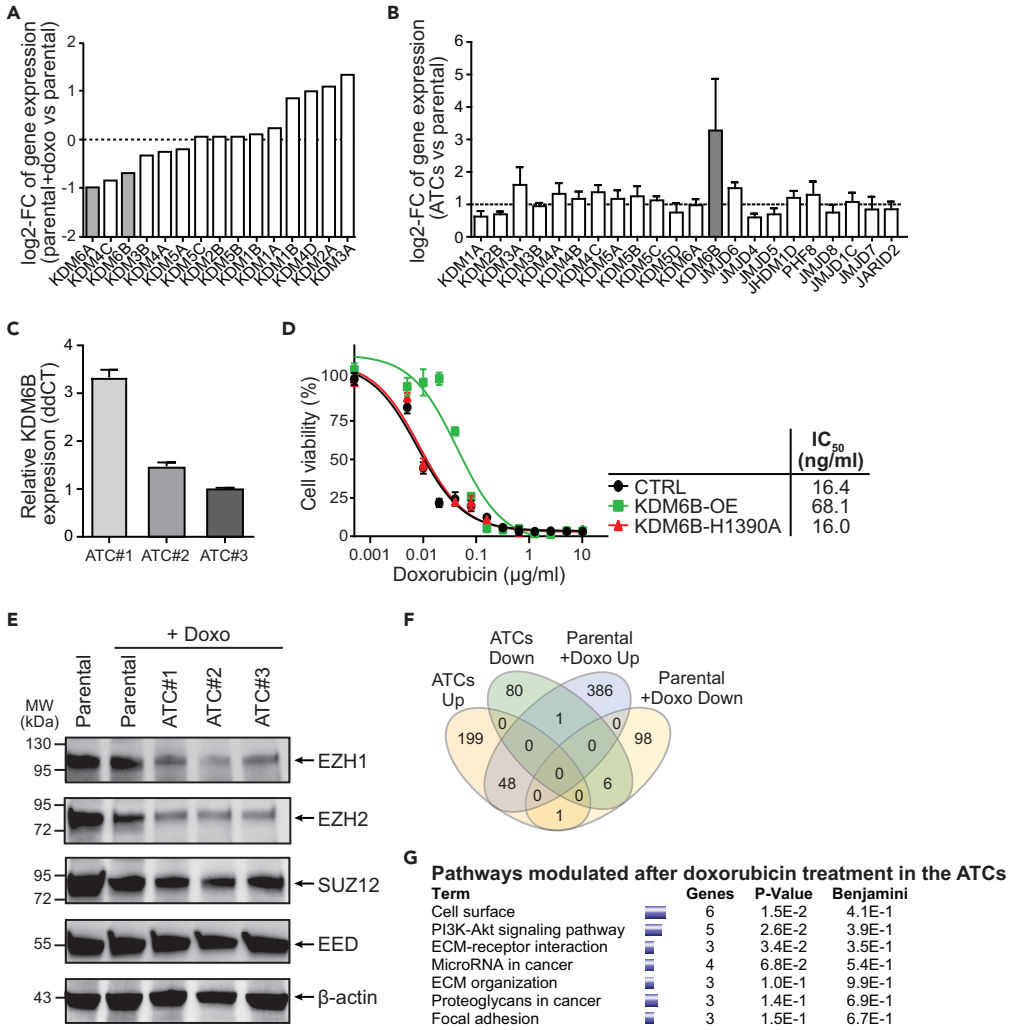

Figure 3. ATCs exhibit enhanced KDM6B and reduced EZH1 and EZH2 expression

(A and B) Expression of demethylases determined using RNA-sequencing and represented as log2 fold-change (FC) expression in (A) K562 parental cells incubated with doxorubicin (225 ng/mL) for 48 h relative to untreated parental cells, and (B) ATCs. For ATCs, data is plotted as mean log2 FC ± SD of ATC#1–3 relative to parental cells.

(C) Relative KDM6B expression in the ATCs as compared with parental cells, measured in duplicate by Q-RT-PCR.

(D) Parental cells were transiently transfected with control (CTRL), KDM6B (KDM6B-OE) or KDM6B-H1390A mutant plasmids. Cell viability of transfected cells treated with doxorubicin for 96 h was measured by MTT (in triplicate) and depicted as value of treated cells relative to untreated cells. Graph is representative of three independently performed experiments.

(E) Immunoblot analysis of EZH1, EZH2, SUZ12, EED and β-actin levels in parental cells treated with or without doxorubicin (225 ng/mL) for 48 h, and ATCs cultured in presence of doxorubicin (225 ng/mL). Immunoblot is representative of three independent experiments.

(F and G) Analyses of overlapping top genes modulated after doxorubicin treatment in the parental cells and ATC#1–3.

(F) Venn diagram showing overlapping genes, which are listed in Table S5.

(G) Pathway analysis, using David, of the overlapping genes.

In the ATCs there is enhanced expression of stem cell markers, regulated by H3K27 and H3K4 methylation marks at their promoter regions

Considering that chemotherapy resistant subpopulations of leukemia cells have been linked to "stemness" and LSCs (Costello et al., 2000; Ho et al., 2016; Ishikawa et al., 2007), we investigated whether doxorubicin induced stem cell genes and whether the ATCs express markers and/or transcriptional programs shared with LSCs. We compared the transcriptional signature of the ATCs with gene expression profiles of AML

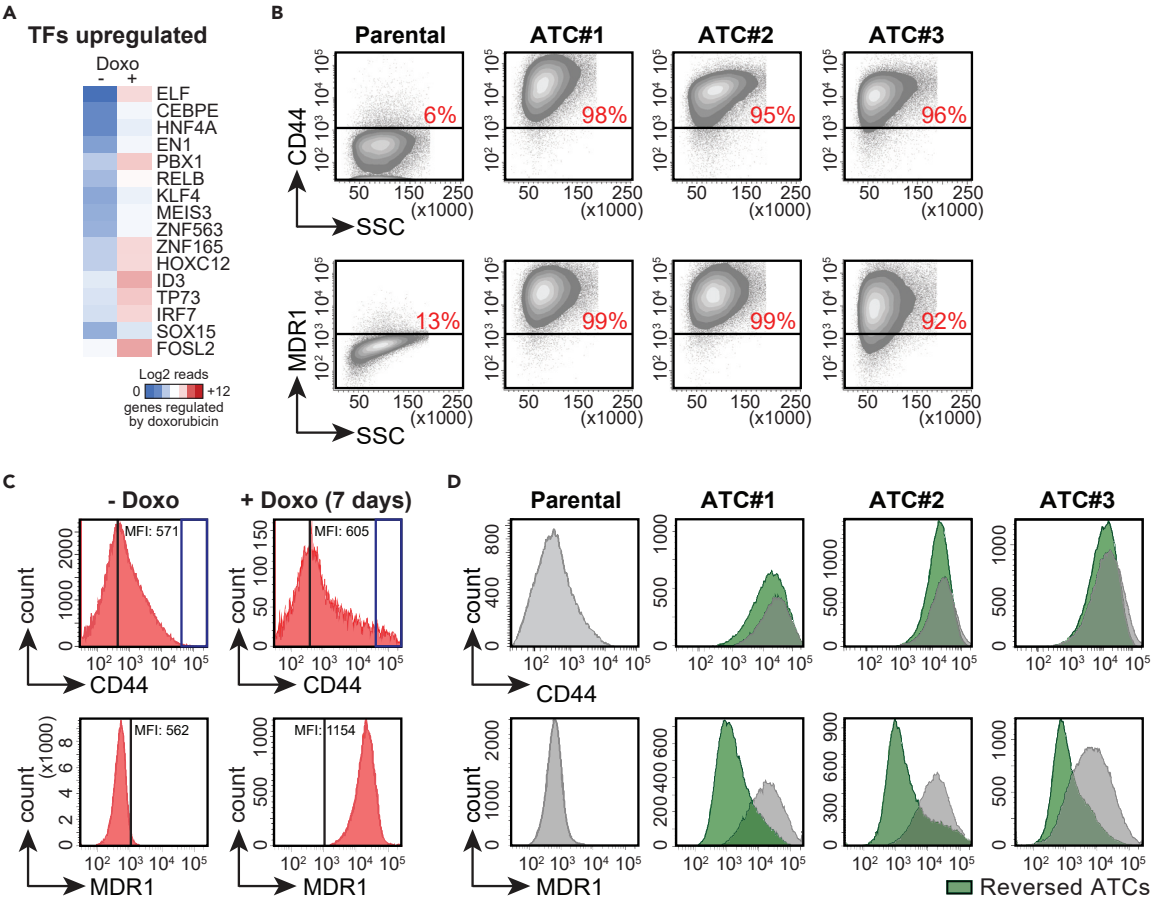
A
TFs upregulated
Doxo
- +
ELF
CEBPE
HNF4A
EN1
PBX1
RELB
KLF4
MEIS3
ZNF563
ZNF165
HOXC12
ID3
TP73
IRF7
SOX15
FOSL2
Log2 reads
0 +12
genes regulated by doxorubicin
B
Parental
ATC#1
ATC#2
ATC#3
CD44
MDR1
SSC
6%
98%
95%
96%
13%
99%
99%
92%
C
- Doxo
+ Doxo (7 days)
MFI: 571
MFI: 605
MFI: 562
MFI: 1154
count
CD44
MDR1
D
Parental
ATC#1
ATC#2
ATC#3
CD44
MDR1
Reversed ATCs
E
40kb
Parental
ATC#1
ATC#2
ATC#3
CD44
F
120kb
MDR1
G
90kb
H3K27me3
H3K4me3
H
120kb

Figure 4. In the ATCs there is enhanced expression of stem cell markers, regulated by H3K27 and H3K4 methylation marks at their promoter regions

(A) K562 parental cells were treated with 225 ng/mL doxorubicin for 48 h, and gene expression profiling (GEP) was performed using RNA-sequencing. Heatmap showing the top upregulated transcription factors (TFs) in parental cells after doxorubicin treatment.

(B and C) Flow cytometric analysis of (B) CD44 and MDR1 membrane expression on ATCs and parental cells, (C) expression of membrane MDR1 and CD44 on parental cells incubated with doxorubicin (225 ng/mL) for 7 days, and (D) membrane CD44 and MDR1 expression on parental cells and ATCs cultured in the presence (gray) and absence (green, reversed-ATCs) of doxorubicin (225 ng/mL) for 10 weeks.

(E and F) Appearing ATAC-sequencing peaks for the (E) CD44 locus and (F) MDR1 locus.

(G and H) ChIP-sequencing tracks showing H3K27me3 and H3K4me3 signals for the (G) CD44 gene and (H) MDR1 gene. P, promoter.

LSCs (Eppert et al., 2011; Gal et al., 2006; Ng et al., 2016), and could only identify an association with downregulated genes in $CD34^{+}CD38^{-}$ AML cells as compared to more differentiated $CD34^{+}CD38^{+}$ AML progenitors (Gal et al., 2006) (Figure S3C).

Several of the TFs upregulated by doxorubicin are known to be involved in inducing "stemness" into cancer cells, including PBX1, KLF4, RELB, ID3 and IRF7 (Figure 4A) (Fang et al., 2020; Ikawa et al., 2015; Lu et al., 2020; Ohtsu et al., 2016; Shimabe et al., 2009; Qadir et al., 2020). Moreover, among the top 25 upregulated genes were *ABCB1*, *CD44* and *CD96* (Figure S2A, arrows), previously shown to be associated with the cancer stem cell phenotype in various tumors, including AML, and resistance to daunorubicin (Hosen et al., 2007; Jin et al., 2006; Patrawala et al., 2005; Williams et al., 2020). Besides enhanced mRNA expression, the ATCs showed elevated expression of membrane CD44 and MDR1 (*ABCB1*) protein on almost 100% of the cells (Figure 4B).

The $CD44^{high}MDR1^{high}$ persisters might have pre-existed before therapy, however, they could also have acquired CD44 and/or MDR1 during treatment. To investigate whether treatment could induce CD44 or MDR1, parental cells were incubated with 225 ng/mL doxorubicin for 7 days and assessed for membrane CD44 and MDR1 expression (Figure 4C). All cells acquired membrane MDR1 after treatment with doxorubicin, whereas on the majority of cells no membrane CD44 was induced. Notably, a small population of cells showed an increase in CD44 (Figure 4C, blue squares), potentially reflecting cells that grew out to become ATCs.

As withdrawal of doxorubicin reversed the drug-tolerant phenotype, we investigated whether expression of CD44 and/or MDR1 returns to similar levels in the ATCs as in parental cells after removal of doxorubicin. On culturing the ATCs without doxorubicin, membrane MDR1 diminished (Figure 4D, bottom), suggesting that the increase in MDR1 is doxorubicin-driven. Notably, and not observed in parental cells, within the reversed-ATC cell population a small $MDR1^{high}$ cell population persisted. On the contrary, CD44 remained stably expressed on the reversed-ATCs (Figure 4D, top), suggesting that CD44 expression is not driven by doxorubicin and that the CD44-positive cells are selected rather than induced by the treatment. To test whether cells with high CD44 have lower sensitivity for anthracyclines than $CD44^{low}$ cells and could have a survival advantage during treatment, we purified $CD44^{high}$ and $CD44^{low}$ K562 cells and incubated these cells with increasing concentrations of doxorubicin (Figure S3D). Indeed, $CD44^{high}$ cells had a 2-fold lower sensitivity for doxorubicin than $CD44^{low}$ cells (IC_{50} of 0.3 μg/mL versus 0.6 μg/mL, respectively), suggesting that rare cells with high membrane CD44 within the bulk of $CD44^{low}$ leukemic cells are more likely to become doxorubicin-resistant during treatment. Because the reversed-ATCs are sensitive to doxorubicin while having CD44 (Figure 4D), we speculate that CD44 is marking a subpopulation of stem cell-like cells with reduced sensitivity to doxorubicin, but that CD44 is not causally involved in the resistance phenotype of the ATCs.

Because low H3K27me3 demonstrated to be associated with therapy resistance (Göllner et al., 2016; Maganti et al., 2018), we investigated whether enhanced MDR1 and CD44 on the ATCs could be the result of modulated H3K27me3, H3K4me3 and an open chromatin state at the promoter regions of these genes. Using the assay for transposase-accessible chromatin using sequencing (ATAC-seq) we showed that both the CD44 and MDR1 locus and promoter region were more open in the ATCs than in parental cells (Figures 4E and 4F), indicative of an active transcriptional state. Using chromatin-immunoprecipitation followed by sequencing (ChIP-seq) we showed that at the CD44 locus there are clearly less repressive H3K27me3 signals at the whole gene and promoter, whereas the active H3K4me3 mark was enhanced at the promoter site in the ATCs compared to parental cells (Figure 4G). A clear increase in H3K27me3 at a region close to the MDR1 promoter but also enhanced H3K4me3 at the promoter locus of MDR1 was observed in the ATCs as compared to parental cells (Figure 4H), suggesting that MDR1 expression is regulated by presence of

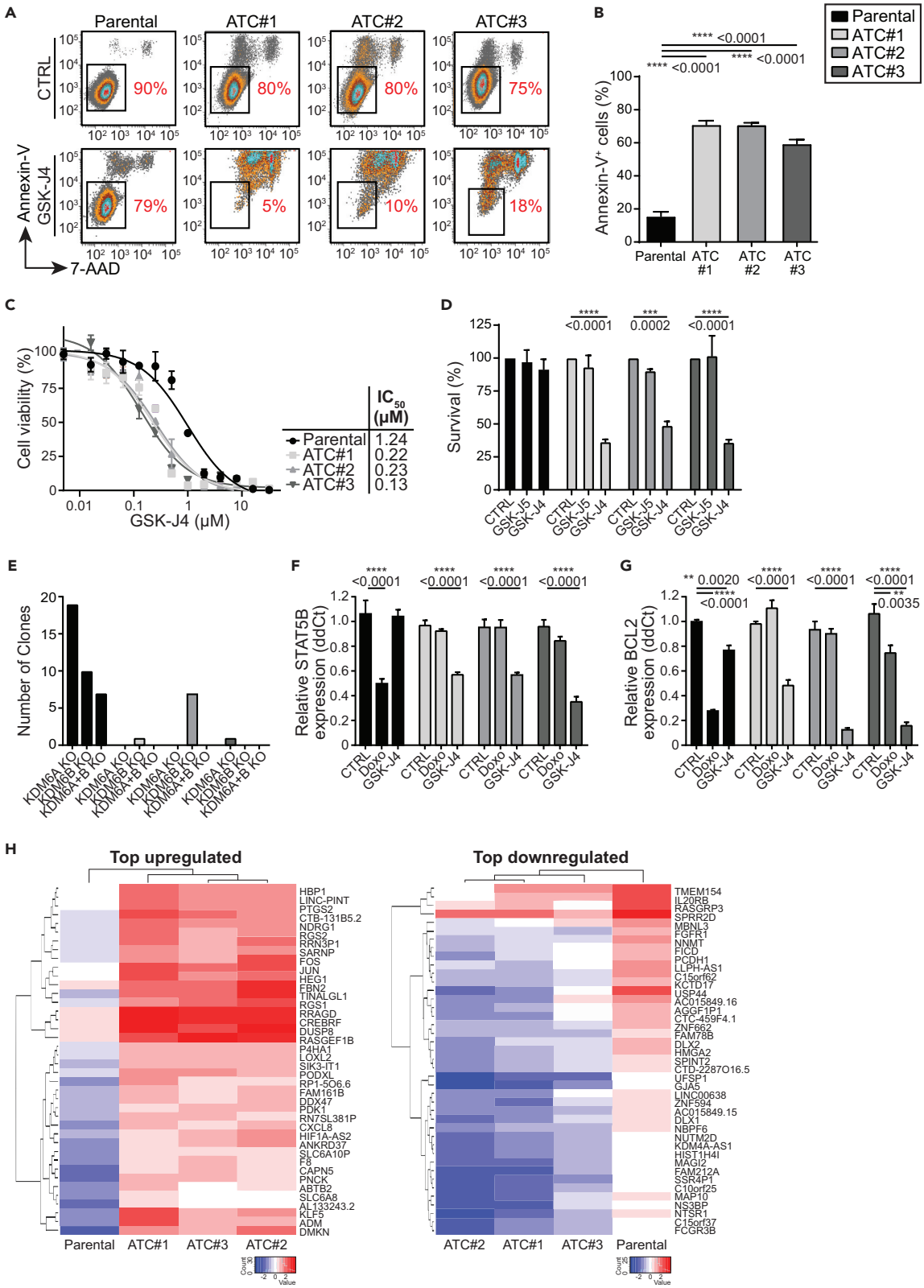
A
Parental
ATC#1
ATC#2
ATC#3
CTRL
Annexin-V
GSK-J4
7-AAD
90%
80%
80%
75%
79%
5%
10%
18%
B
Parental
ATC#1
ATC#2
ATC#3
Annexin-V+ cells (%)
Parental
ATC #1
ATC #2
ATC #3
C
Cell viability (%)
GSK-J4 (μM)
IC50 (μM)
Parental 1.24
ATC#1 0.22
ATC#2 0.23
ATC#3 0.13
D
Survival (%)
CTRL
GSK-J5
GSK-J4
E
Number of Clones
KDM6A KO
KDM6B KO
KDM6A+B KO
F
Relative STAT5B expression (ddCt)
CTRL
Doxo
GSK-J4
G
Relative BCL2 expression (ddCt)
H
Top upregulated
Top downregulated
Parental
ATC#1
ATC#3
ATC#2

Figure 5. Reprogramming the transcriptional state by enhancing histone methylation depletes the anthracycline-tolerant persisters

For all assays, cell viability and gene expression is depicted as value of GSK-J4 or GSK-J5 treated cells (96 h) relative to untreated (CTRL) cells. p-values were determined using a two-way ANOVA and post-hoc Dunnett's multiple comparison test unless stated otherwise.

(A and B) ATCs and parental cells were treated with 2 μM GSK-J4, stained with Annexin-V and 7-AAD and measured using flow cytometry.

(A) Representative experiment, gates indicate the percentage of viable cells.

(B) Induction of apoptosis as depicted by the percentage of Annexin-V^+ cells. p-values were determined by a one-way ANOVA and post-hoc Tukey's multiple comparison test.

(C and D) Cell viability, measured using MTT, of ATCs and parental cells treated with (C) GSK-J4, shown as representative graph of two independently performed experiments (in triplicate), and (D) 1 μM GSK-J5 or 1 μM GSK-J4, plotted as mean ± SD.

(E) The number of clones that survived knock-out of KDM6A (KDM6A-KO), KDM6B (KDM6B-KO) or the combination (KDM6A + B KO) using CRISPR-Cas9 transduction.

(F and G) Expression of (F) STAT5B and (G) BCL2 in parental cells and ATCs treated with 300 ng/mL doxorubicin or 1 μM GSK-J4 for 7 days, measured by Q-RT-PCR and plotted as mean ± SD.

(H) Heatmap of hierarchically clustered top 40 genes up- and downregulated between ATCs and parental cells after treatment with 1 μM GSK-J4 for 72 h, measured using RNA-seq. Genes were selected based on their log2 fold-change expression.

histone modifications associated with both gene activation and repression at or close to the promoter, a so called a poised state, which is often observed at promoters of genes expressed in stem cells (Bernstein et al., 2006).

Reprogramming the transcriptional state by enhancing histone methylation depletes the anthracycline-tolerant persisters

Next, we aimed at either inducing sensitivity for doxorubicin or apoptosis by transcriptionally reprogramming the therapy-tolerant state. We choose the approach of enhancing H3K27me3 levels by inhibition of KDM6 using the inhibitor GSK-J4 (Kruidenier et al., 2012). GSK-J4 treatment reduced viability of ATC#1-3 cells, by inducing apoptosis, with a 5 to 10-fold higher sensitivity than it did in the parental cells (Figures 5A–5C). To demonstrate that the effect is specific for inhibition of KDM6 activity, we treated the ATCs with GSK-J5, an inactive GSK-J4 isomer lacking KDM6 binding capacity (Kruidenier et al., 2012), and showed that GSK-J5 did not affect survival of the ATCs (Figure 5D). No increase in sensitivity for doxorubicin or decrease in membrane MDR1 after GSK-J4 treatment was observed (data not shown), indicating that GSK-J4 directly induced apoptosis specifically in the ATCs.

To further investigate whether there is dependency of the ATCs on KDM6 demethylases we applied a knockdown strategy using siRNAs directed against KDM6A and KDM6B (Figures S3E and S3F). Downregulation of KDM6A or KDM6B led to reduced survival of ATC#1 and ATC#3, whereas the parental cells were not affected (Figure S3G). Similar to GSK-J4, reducing KDM6 by siRNAs in the ATCs did not affect the sensitivity for doxorubicin (data not shown). Moreover, knocking-out KDM6A or KDM6B or both using CRISPR-Cas9 (Figure S3H) resulted in less surviving clones from the ATCs than from the parental cells depleted for KDM6A and/or KDM6B (Figure 5E). All surviving clones had a deletion, frameshift or stop codon at the position of the gRNAs (Figure S3I), resulting in reduced expression of KDM6A and/or KDM6B (Figure S3J). ATC clones that survived knock-out of KDM6 showed a similar growth rate as parental cells lacking KDM6, except for ATC#3 clone #1 lacking KDM6A (Figure S3K). Together, these results suggest that the ATCs are more dependent on KDM6 activity than the parental cells, however that there is a heterogeneous dependency within the cell populations of both parental cells and ATCs.

Treatment of the parental cells with doxorubicin led to decreased STAT5B levels, whereas it did not in the ATCs (Tables S2, S3, and S4). As STAT5B, but also BCL2, are involved in induction of apoptosis, we hypothesized that downregulation of STAT5B and BCL2 might be markers of a good response, and that GSK-J4 treatment might specifically reduce STAT5B and BCL2 levels in the ATCs. Indeed, although doxorubicin reduced STAT5B and BCL2 in the parental cells and not in the ATCs, GSK-J4 efficiently reduced expression of STAT5B and BCL2 in the ATCs but not in the parental cells (Figures 5F and 5G).

Thus, epigenetic reprogramming by GSK-J4 efficiently eradicated the ATCs. To identify biomarkers indicative of an effective GSK-J4 response we searched for genes changed after treatment in the ATCs but not in parental cells (Figure 5H). Pathway analysis showed that treatment of the ATCs with GSK-J4 changed the expression of factors linked to epigenetic mechanisms, including regulation of gene expression and TF binding and activity (Figure S4A). Protein-protein interaction analysis revealed that the TFs Fos and Jun are central proteins upregulated after GSK-J4 treatment in the sensitive cells,

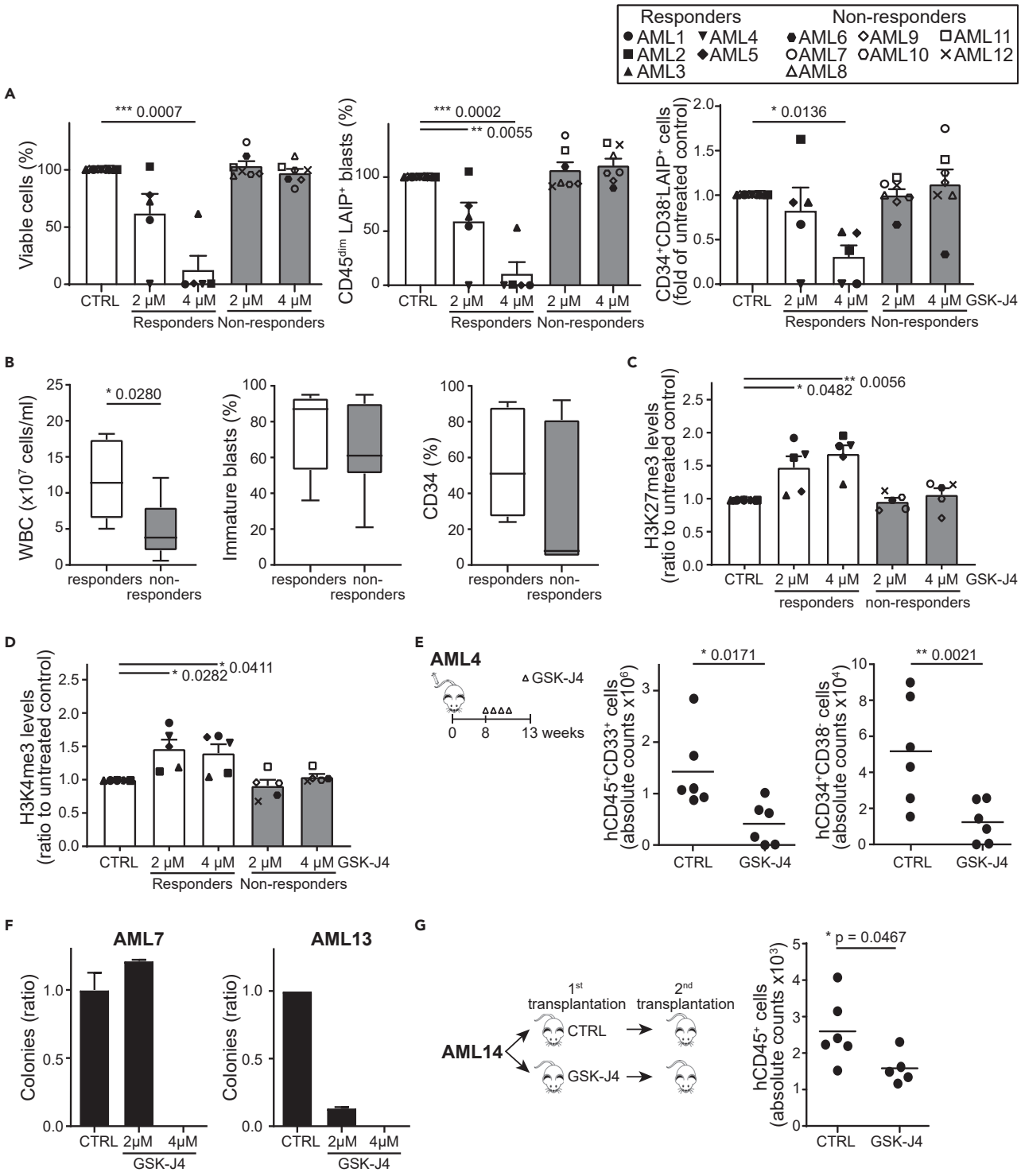

Figure 6. GSK-J4 eradicates AML stem cells *ex vivo* and *in vivo*

Patient characteristics are summarized in Table S6. p-values were determined using a Student's *t* test unless stated otherwise.

(A–D) Primary AML cells of patients at diagnosis (n = 12) were treated with GSK-J4 and evaluated according to their response; responders (n = 5) and non-responders (n = 7). (A) Percentage of viable cells (left), leukemic $CD45^{dim}LAIP^{+}$ blasts (middle) and $CD34^{+}CD38^{-}LAIP^{+}$ cells (right) after 4 days of GSK-J4 treatment, measured using flow cytometry, quantified relative to flow count beads, normalized against untreated controls (CTRL) and plotted as mean ± SEM p-values were determined using a one-way ANOVA with post-hoc Tukey's multiple comparison test.

Figure 6. *Continued*

(B) White blood cell (WBC) count (left), percentage of myeloid immature $CD45^{dim}$ blasts in total WBC (middle) and the percentage of $CD34^+$ on blasts cells (right).

(C and D) Quantification of immunoblot analysis of (C) H3K27me3 and (D) H3K4me3 expression levels. For each individual primary AML sample, protein levels were normalized against β-actin levels and depicted as ratio to untreated controls (CTRL).

(E) Schematic overview of the experiment (left). After injection of T cell depleted primary AML4 cells, NSG mice were treated four times with 10 mg/kg GSK-J4 in week 8 (days 1–4). At week 13, mice bone marrows were analyzed for the presence of human myeloid $hCD45^+CD33^+$ (middle) and $CD34^+CD38^-$ (right) cells.

(F) Colony forming unit assay (duplicate) of 2 AML patients at diagnosis after treatment with GSK-J4 and cultured for 7 days. The control sample (CTRL) was set to 1.

(G) Schematic overview of the experiment (left). After injection of T cell depleted primary AML14 cells, NSG mice (first recipients) were treated with PBS (CTRL) or 15 mg/kg GSK-J4 in week 10 (days 1, 3, 7) and week 13 (days 1, 4, 7). Equal numbers of human myeloid $CD45^+CD33^+$ cells derived from the first transplant, isolated in week 16, were injected into secondary recipients. At week 19, spleens of secondary mice were analyzed for the presence of human $CD45^+$ cells (right).

suggesting a role for these TFs in reprogramming the transcriptome by GSK-J4 and driving apoptosis (Figure S4B).

GSK-J4 eradicates AML stem cells *ex vivo* and *in vivo*

Treatment of AML cell lines with GSK-J4 showed only an efficient response in the relative daunorubicin-resistant KG1 and Kasumi-1 cell lines (Figure S4C) (Rao et al., 2011), suggesting a negative correlation between sensitivity to anthracylines and GSK-J4 in AML. Next, we assessed the sensitivity to both doxorubicin and GSK-J4 in twelve primary AML cases (Table S6). Five out of 12 patients showed a good response to GSK-J4, demonstrated by a significant reduction in total viable cells, leukemic blasts ($CD45^{dim}$ cells expressing a leukemia-associated immunophenotype (LAIP) (Feller et al., 2013)) and a reduction in immature $CD45^{dim}CD34^+CD38^-LAIP^+$ leukemic cells (Figure 6A, example responder Figure S4D), with IC_{50} values ranging from 1.1 to 4.0 μM (measured in 4/5 responders; Figure S4E). No correlation of GSK-J4 sensitivity and *ex vivo* response to doxorubicin was observed in these AML diagnosis samples (Figure S4F). However, comparing clinical features, molecular aberrancies and cytogenetics of responders and non-responders showed that in the responders there are slightly more $CD34^+$ leukemia cells (mean of 56.2% and non-responders mean of 38.4%), more immature blasts (mean of 75.8%, and non-responders mean of 65.6%) and significantly more white blood cells (WBC) (mean of 118.3×10^6 cells/mL and non-responders mean of 48.0×10^6 cells/mL) (Figures 6B, S4G, and Table S6), suggesting that GSK-J4 is efficient in AML cases that have a high WBC count and a poor response to combination chemotherapy (Rollig and Ehninger, 2015; Walter et al., 2015).

Four out of 5 responders showed clear upregulation of H3K27 and/or H3K4 methylation after GSK-J4 treatment, whereas H3K27me3 and H3K4me3 levels were unaffected in all non-responders (Figures 6C, 6D, S5A). The basal levels of H3K27me3 and/or H3K4me3 were similar in responders and non-responders (Figures S5B and S5C). Moreover, we did not observe a significant difference in KDM6A, KDM6B, EZH1 and EZH2 expression levels between GSK-J4 responders and non-responders (Figures S5D–S5G). Altogether, these results suggest that response to GSK-J4 is associated with the capacity to enhance H3K27me3 and/or H3K4me3 levels.

To evaluate whether treatment with GSK-J4 can deplete poor prognosis AML *in vivo*, primary AML cells of a patient with high WBC (114×10^6 cells/mL) were transplanted into NSG mice, and after leukemia appeared in the blood the mice were treated with 10 mg/kg GSK-J4 for four times (Figure 6E). A significant reduction in total human $CD45^+$ blasts (Figure S5H), human myeloid leukemia cells and immature human immature leukemic $CD45^+CD34^+CD38^-$ cells in the mice bone marrows was observed after GSK-J4 treatment as compared to controls (Figure 6E). Moreover, treatment with GSK-J4 reduced self-renewal capacity of LSCs/leukemic progenitors residing within diagnosis AML, demonstrated by a reduction in number of colonies in AML13 (at 2 μM) and AML 7 (at 4 μM) (Figure 6F). Although AML7 is annotated as a non-responder because there was no reduction in immunophenotypically defined blasts (Figures 6A and S4G), GSK-J4 efficiently eliminated clonogenic leukemic stem/progenitors from the AML7 bone marrow (Figure 6F). To study the effect of GSK-J4 on LSC survival *in vivo*, we performed secondary transplantations in immunodeficient mice. Equal numbers of viable human AML cells from first transplanted mice (AML14) treated with GSK-J4 (6×15 mg/kg) or PBS were injected into secondary recipients. Treatment with GSK-J4 significantly reduced secondary engraftment of human $CD45^+$ AML cells (Figure 6G), suggesting that part of functionally defined LSCs are depleted by treatment with GSK-J4.

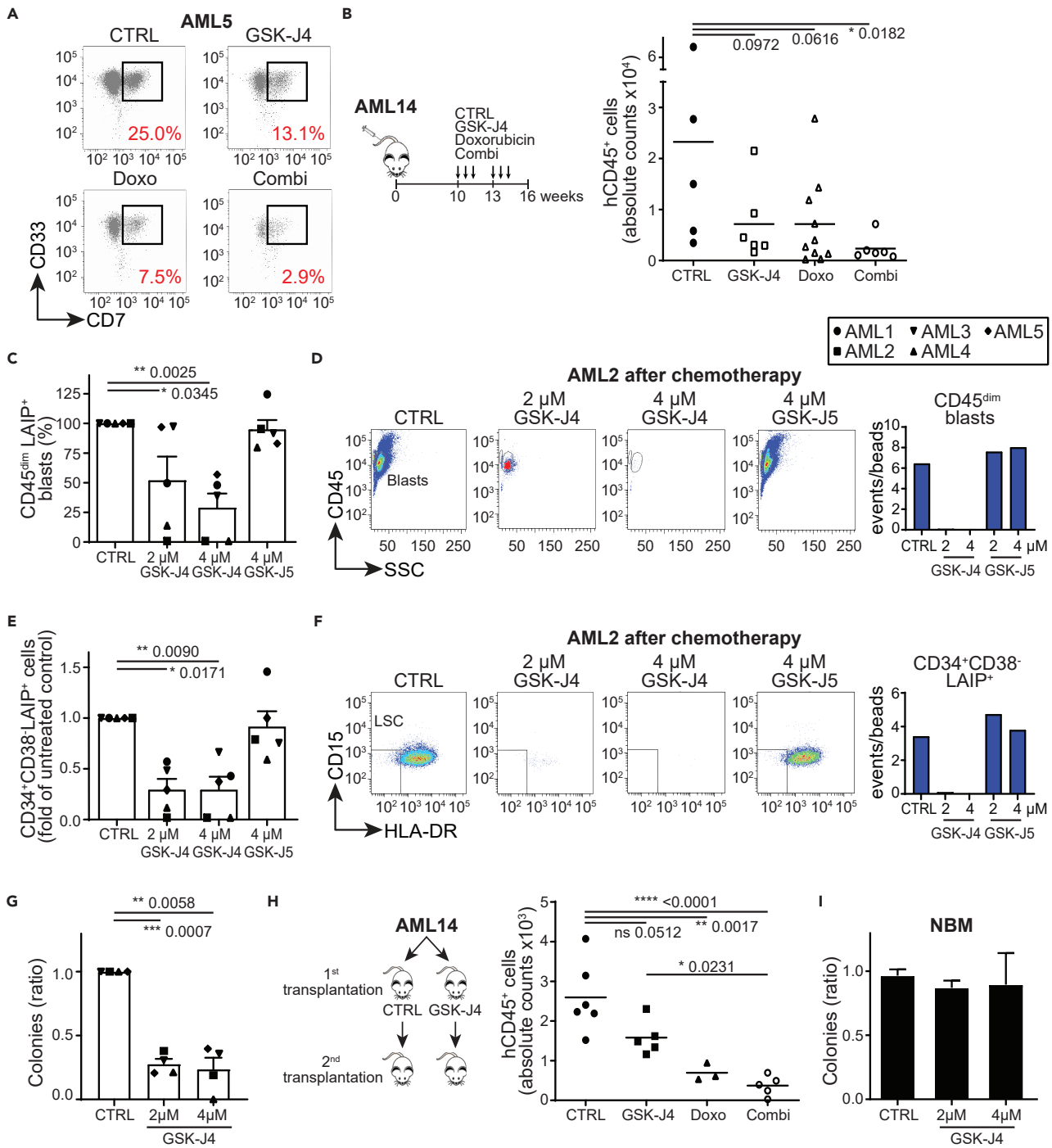

Figure 7. GSK-J4 treatment eradicates AML MRD, and leukemic stem/progenitor cells residing within MRD, while sparing normal stem/progenitor cells

Patient characteristics are summarized in Table S6. Colony forming unit assays were performed after treatment of cells with GSK-J4 for 7 days, and for each individual sample the control (CTRL) was set at 1. p-values were determined using a one-way ANOVA with post-hoc Tukey's multiple comparison test unless stated otherwise.

(A) Percentage of viable $CD45^{dim}CD33^{+}LAIP^{+}$ ($CD7^{+}$) primary AML cells after treatment with 10 ng/mL doxorubicin, 3 µM GSK-J4, or the combination (doxorubicin treatment at days 1–3 and GSK-J4 treatment at days 4–7), measured using flow cytometry and quantified relative to flow count beads.

Figure 7. *Continued*

(B) Schematic overview of the experiment (left). After injection of T cell depleted primary AML14 cells, NSG mice were treated with PBS (CTRL), 15 mg/kg GSK-J4, 1.5 mg/kg doxorubicin, or the combination in week 10 (days 1, 3, 7) and/or week 13 (days 1, 4, 7). At week 16, mice bone marrows were analyzed for presence of human $CD45^+$ (right) cells. p-values were determined using a one-way ANOVA with post-hoc Dunnett's multiple comparison test.

(C–F) AML residual disease ($LAIP^+$ leukemia) samples derived from patients treated with combination chemotherapy (n = 5) were incubated with GSK-J4 and GSK-J5 for 7 days. Samples were measured using flow cytometry, quantified relative to flow count beads and normalized against untreated controls (CTRL).

(C) Percentage of $CD45^{dim}LAIP^+$ blasts. (D) Example of AML2 incubated with GSK-J4, showing viable $CD45^{dim}$ blasts. (E) Percentage of $CD34^+CD38^-LAIP^+$ cells. (F) Example of AML2 incubated with GSK-J4, showing viable $CD34^+CD38^-CD15^+HLA\text{-}DR^-$ LSCs.

(G) Colony forming unit assay (duplicate) of AML residual disease cells, derived from patients treated with combination chemotherapy (n = 4).

(H) Schematic overview of the experiment (left). Equal numbers of human $CD45^+CD33^+$ AML14 cells derived from the first transplant (as described in B) were injected into secondary recipients. At week 19, spleens of secondary mice were analyzed for the presence of human $CD45^+$ cells (right).

(I) Colony forming unit assay of normal bone marrow (NBM) cells from a healthy donor.

GSK-J4 treatment eradicates AML MRD, and leukemic stem/progenitor cells residing within MRD, while sparing normal stem/progenitor cells

To investigate whether GSK-J4 treatment could reduce primary AML cells that have survived chemotherapy, we incubated an AML sample with doxorubicin and subsequently with GSK-J4. Inhibition of KDM6 by GSK-J4 could reduce the viability of myeloid leukemia blasts ($CD45^{dim}CD33^+CD7^+$ cells) that survived the doxorubicin treatment *ex vivo* by 2.6-fold (Figure 7A). Moreover, combination treatment of doxorubicin and GSK-J4 resulted in a significant reduction of leukemia load in mice transplanted with primary AML cells of a patient with high WBC (140×10^6 cells/mL), while the monotherapies did not (Figure 7B).

Chemotherapy-resistant leukemia cells that survived treatment in AML patients constitute MRD. MRD, and LSCs residing within MRD, are thought to be at the origin of relapse (Ossenkoppele and Schuurhuis, 2016; Terwijn et al., 2013). To investigate whether transcriptional reprogramming by GSK-J4 could eliminate or reduce MRD load, we incubated AML residual disease ($LAIP^+$ leukemia cells) derived from patients treated with combination chemotherapy (cytarabine and an anthracycline) (n = 5) with GSK-J4. GSK-J4 treatment resulted in a significant reduction in leukemic $CD45^{dim}LAIP^+$ blasts from these patient samples at the stage of MRD (Figures 7C and 7D), suggesting that GSK-J4 treatment is able to reduce AML MRD load. Notably, in AML2 and AML4, GSK-J4 completely eliminated the residual leukemic blasts (Figure 7C).

LSCs are changing during the course of the disease (Boyd et al., 2018), and responsible for relapse initiation. We therefore investigated, in addition to the efficiency of GSK-J4 to eliminate LSCs at diagnosis (Figures 6F and 6G), the potential of GSK-J4 to deplete leukemic stem/progenitor cells from MRD. A significant reduction in immature $CD45^{dim}CD34^+CD38^-LAIP^+$ LSCs was observed after GSK-J4 treatment of residual disease from patients treated with combination chemotherapy (n = 5) (Figures 7E and 7F). Moreover, a reduction in the number of colonies was observed when AML MRD patient samples (n = 4) were treated with GSK-J4 (Figures 7G and S5I), implicating that leukemic progenitors residing within MRD are efficiently eliminated by GSK-J4. To validate that GSK-J4 treatment depleted progenitors that are leukemic, we collected the colonies from the control samples and showed that >90% had a molecular mutation, a NPM1-mutation and/or a FLT3-ITD, and >90% of the colony-derived $CD45^{dim}$ blast cells had expression of an LAIP (data not shown). To elucidate whether GSK-J4 could eradicate LSCs that survive doxorubicin treatment, we re-transplanted equal numbers of AML cells derived from first transplanted mice treated with either doxorubicin, GSK-J4, or the combination into secondary recipients, and showed that GSK-J4 could enhance chemotherapy-induced LSC death *in vivo* (Figure 7H).

GSK-J4 specifically eliminated leukemic cells, as it did not affect colony forming capacity of stem/progenitor cells within healthy bone marrow (Figure 7I). The differential effect of GSK-J4 on malignant versus normal healthy cells might be because of the differential expression of KDM6 between AML and normal immature cells such as hematopoietic stem cells (HSCs), multipotent progenitor cells (MPP), common myeloid progenitor cells (CMP), granulocyte monocyte progenitors cells (GMP) and megakaryocyte-erythroid progenitor cells (MEPs) (Li et al., 2018).

DISCUSSION

Insufficient eradication of a small subpopulation of leukemic cells that survived initial chemotherapy treatment, and that is able to re-initiate leukemia, is the main reason for the poor survival rates of AML patients. Although much progress has been made in understanding genetically induced intra-tumoral heterogeneity

underlying different sensitivities to chemotherapy (Ding et al., 2012), knowledge with respect to enhanced drug tolerance induced by epigenetic mechanisms is limited. Here, we report on the identification of a rare subpopulation of leukemia persisters that are in a transient anthracycline-resistant state. The resistant state was forced onto the cells by presence of the drug, indicating that it is likely that the treatment itself induced transcriptomic and epigenomic changes into the leukemia cells, resulting in a dynamic doxorubicin-tolerant state. AML-initiating cells within a patient are transcriptionally heterogeneous at the single cell level, which might facilitate the evolution of these cells on treatment with chemotherapy (Stetson et al., 2021). Anthracyclines might select for specific gene expression programs among leukemia cells that might facilitate treatment escape and resistance. Of note, the transcriptional state of AML cells during the disease course is dynamic (Boyd et al., 2018). In this study, we have focused on a fixed transcriptional state under drug pressure, but it will be of interest to assess the transition of leukemia cells under pressure of therapy by single-cell RNA sequencing. Whether the resistant cells have altered epigenomes and represent a selected subpopulation of treatment naive cells or whether they have emerged following treatment could also be elucidated from these single-cell RNA sequencing studies. The altered gene expression programs and a modulated chromatin-state in the ATCs might have been co-opted in drug resistance by inhibition of apoptosis. Recently, it has been indeed demonstrated that during AML progression there is, next to DNA clonal evolution, RNA clonal evolution involving metabolism, apoptosis and chemokine signaling (Stetson et al., 2021). We here showed that $CD44^{high}$ cells have a decreased sensitivity to doxorubicin and therefore have a higher chance to growth out under drug pressure. Notably, at AML relapse there is enhanced expression of CD44 as compared to AML diagnosis (Stetson et al., 2021).

We identified that the ATCs have a lack of upregulating H3K27me3 after doxorubicin treatment. An aberrant epigenetic state due to low levels of H3K27me3 in tumor cells or in a small subpopulation of cells within the tumor has been previously observed in different cancer types and has been correlated with reduced treatment response (Göllner et al., 2016; Maganti et al., 2018). In AML patients, KDM6B is overexpressed, and high expression is associated with a poor prognosis (Boila et al., 2018; Li et al., 2018). Moreover, loss of the PRC2 components MTF2, EED, SUZ12 and EZH2 resulted in chemotherapy resistance (Maganti et al., 2018; Xie et al., 2014). Both EZH1 and EZH2 are reduced in the ATCs, which is consistent with the observation that chemotherapy resistance is only achieved when both EZH1 and EZH2 are inhibited (Maganti et al., 2018). We showed that leukemia cells with enhanced KDM6B activity are less sensitive to doxorubicin. Together, this made us hypothesize that the leukemia cells with a resistant phenotype and low levels of H3K27me3, because of either enhanced KDM6 and/or decreased EZH1/2, might be sensitive to upregulation of H3K27 methylation by KDM6 inhibition. Indeed, GSK-J4 specifically reduced cell viability of the ATCs, suggesting that anthracycline-tolerant leukemia cells require low H3K27me3 and an altered chromatin state to persist. Previously, KDMs demonstrated to play a role in maintaining transcriptional plasticity during progression toward drug resistance in lung cancer and glioblastoma (Dalvi et al., 2017; Liau et al., 2017), and also in pediatric brainstem gliomas harboring a dominant-negative oncogenic K27M mutation of histone H3.3, inhibition of KDM6 induced apoptosis by increasing H3K27 methylation (Hashizume et al., 2014).

One of the best characterized mechanisms of anthracycline resistance is increased membrane expression of MDR1. High MDR1 correlates with poor response to chemotherapy and a dismal outcome for AML patients (Leith et al., 1999; Sato et al., 1990). Chemotherapy activates an integrated stress-response-like transcriptional program to induce MDR1 through modeling and activation of an ATF4-bound, stress-responsive enhancer (Williams et al., 2020). Because clinical trials testing MDR1 inhibition showed disappointing results (Shaffer et al., 2012), we hypothesized that reprogramming the transcriptional state of the persisters by induction of H3K27 and/or H3K4 methylation might result in induction of apoptosis. We chose the approach of inhibiting KDM6 using GSK-J4 (Kruidenier et al., 2012), and showed that anthracycline-tolerant myeloid leukemia cells are more dependent on KDM6 activity than anthracycline-sensitive parental cells. Of clinical interest is the increased expression of CD44 on the ATCs as CD44 is an adhesion molecule highly expressed on LSCs (Jin et al., 2006), and shown to cooperate with the CXCR4 chemokine receptor for the survival of normal HSCs residing in the bone marrow microenvironment, where its ligand hyaluronan is expressed (Avigdor et al., 2004) (Gal et al., 2006). Activation of CXCR4 by its ligand CXCL12 induced "stemness" onto AML cells, which is dependent on CD44 signaling, and resulted in resistance to venetoclax (Yu et al., 2021). Solely targeting CD44 might not sensitize cells to anthracyclines, but might impact on their "stemness", and in combination with an additional drug might sensitize LSCs to go into apoptosis.

During chemotherapy treatment the frequency and the phenotype of LSCs can change, suggesting that there is plasticity of stem cell-like leukemia cells during the course of the disease (Boyd et al., 2018; Ho et al., 2016). In LSCs within chronic myeloid leukemia there is extensive reprogramming of H3K27 methylation targets (Scott et al., 2016), but AML LSCs also contain altered epigenetic programs (Jung et al., 2015).

Here, we showed that reprogramming the transcriptional state of anthracycline-resistant cells by enhancing H3K27 and/or H3K4 methylation might be a strategy to selectively induce depletion of leukemic progenitor/stem cells that are residing within MRD, as normal stem/progenitor cells were spared. The higher expression of KDM6 in LSCs as compared to normal immature cells and HSCs could be the cause for this selectivity (Li et al., 2018). Also, in breast and ovarian cancer, KDM6 inhibition effectively eradicated cancer stem cells (Sakaki et al., 2015; Xun et al., 2017). In contrast to our results, loss of KDM6B in mouse cells compromised self-renewal of both normal and LSCs (Mallaney et al., 2019). This discrepancy might be explained by a different function of KDM6B in human HSCs as compared with mouse HSCs; however, it might also be that a complete loss of KDM6B in human HSCs is compromising self-renewal and survival, whereas just a reduction in activity is not. This hypothesis is confirmed by the fact that 50% reduction in KDM6B could be deleterious for leukemia-initiating cells, without being toxic to normal HSCs (Mallaney et al., 2019).

Our study is the first description that epigenetic reprogramming could efficiently eradicate AML MRD cells and LSCs residing within MRD, suggesting that inherent plasticity as possible mechanism of tolerance to chemotherapy in MRD and LSCs can be redirected by epigenetic reprogramming to initiate apoptosis. GSK-J4 AML responders have a higher WBC than non-responders, and on treatment showed upregulation of H3K27 and/or H3K4 methylation. Upregulation of H3K4 methylation by GSK-J4 suggests that this inhibitor efficiently inhibits, next to KDM6, H3K4 demethylases. Indeed, GSK-J4 was not only shown to target KDM6 but also the H3K4 demethylases KDM5B and KDM5C (Heinemann et al., 2014).

In the ATCs, upregulation of histone methylation coincides with transcriptional reprogramming, inducing changes in expression of proteins involved in histone binding, TFs, chromatin silencing and activation, and telomere organization, likely indicating that KDMs have both histone and non-histone targets. Indeed, in mouse HSCs, depletion of KDM6 induced a stress response signature, including upregulation of Fos and Jun (Mallaney et al., 2019). Treatment of the ATCs with GSK-J4 also induced Fos and Jun, however, next to those genes several other genes involved in chromatin functioning were modulated.

Recently, application of GSK-J4 was reported in diagnosis AML (Boila et al., 2018). Moreover, GSK-J4 demonstrated effective inhibition of cell survival and cell-cycle progression in Kasumi-1, KG-1 and KG-1a AML cell lines (Li et al., 2018) (Chu et al., 2020). In contrast to our results, GSK-J4 treatment of Kasumi-1 cells led to downregulation of genes related to cell-cycle phase transition and DNA replication, and a decrease in mRNA levels of HOXA5, HOXA7, HOXA9 and HOXA11 (Li et al., 2018). This discrepancy in target genes might be because of the fact that we are comparing sensitive and resistant leukemia cells, and that the identified genes might therefore represent better biomarkers of GSK-J4 response. Our finding that GSK-J4 will add to the nowadays applied combination chemotherapy in AML patients is consistent with results showing that GSK-J4 has a synergistic effect with cytarabine to inhibit AML colony forming capacity (Li et al., 2018), but also that application of GSK-J4 can sensitize diffuse large B-cell lymphoma to chemotherapeutic drugs such as doxorubicin, bortezomib and vorinostat (Mathur et al., 2017).

This study revealed novel insights in reversible anthracycline resistance and provide a rationale to further explore inhibitors directed to histone demethylases, in combination with current chemotherapy regimens, in AML patients, aiming at decreasing AML MRD. This is particularly important as there is a need for more effective therapeutic interventions that improve remission rates and prevent disease recurrence.

Limitations of study

This study used the chronic myelogenous leukemia (CML) cell line K562. Although the K562 cell line is a CML in blast crisis resembling AML cells closely, it expresses the fusion gene BCR-ABL and is therefore not the optimal model system to study AML therapy resistance. In addition, development of MRD after combination chemotherapy in the patient is the sum of all resistance mechanisms against anthracyclines and cytarabine, and does not exactly resemble the ATCs which are only resistant to anthracyclines.

Reprogramming the transcriptional state by targeting KDM6 led to apoptosis of resistant leukemia cells however did not result in upregulation of sensitivity to doxorubicin, suggesting that the transcriptional state of the ATCs is not the direct cause of doxorubicin resistance but drives survival in these cells. Future studies that examine a broader panel of AML cell line-derived resistant clones to both anthracyclines and cytarabine may reveal promising treatment strategies eliminating MRD in AML patients.

STAR★METHODS

Detailed methods are provided in the online version of this paper and include the following:

- KEY RESOURCES TABLE
- RESOURCE AVAILABILITY
  - Lead contact
  - Materials availability
  - Data and code availability
- EXPERIMENTAL MODEL AND SUBJECT DETAILS
  - Animals
  - Cell lines, cell culture and isolation of ATCs
  - Primary AML cell cultures
- METHOD DETAILS
  - Cell viability assays
  - Immunoblotting
  - RNA isolation and Q-RT-PCR
  - Immunostaining and flow cytometry analysis
  - Liquid culture- and colony forming unit assay
  - AML patient-derived xenograft model
  - siRNA knockdown
  - CRISPR-Cas9 induced knockout of KDM6A and KDM6B
  - Transient transfection to overexpress KDM6B
  - RNA sequencing
  - ChIP-sequencing
  - ATAC-sequencing
  - Molecular diagnostics and cytogenetic analysis
- QUANTIFICATION AND STATISTICAL ANALYSIS

SUPPLEMENTAL INFORMATION

Supplemental information can be found online at https://doi.org/10.1016/j.isci.2022.105013.

ACKNOWLEDGMENTS

This study was supported by grants from the Dutch Cancer Society (KWF grant no. 12805) and the Foundation "De Drie Lichten" in the Netherlands (grant no. 52/18).

AUTHOR CONTRIBUTIONS

Conceptualization, N.v.G., H.J.M.P.V., and L.S.; Methodology, N.v.G., H.J.M.P.V., M.B., T.M., F.D., E.V., A.R., T.C., M.C., and M.A.; Formal Analysis, SD and R.X.M.; Investigation, N.v.G., H.J.M.P.V., M.B., T.M., F.D., E.V., A.R., T.C., M.C., and M.A.; Resources, J.J.W.M. and G.J.O.; Writing – Original Draft, N.v.G., H.J.M.P.V., and L.S.; Writing – Review & Editing, M.B., J.C., J.J.W.M., and G.J.O.; Visualization, N.v.G. and H.J.M.P.V.; Supervision, J.C. and L.S.; Funding acquisition, N.v.G. and L.S.

DECLARATION OF INTERESTS

The authors declare no competing interests, and we have full data availability.

Received: May 13, 2022
Revised: June 20, 2022
Accepted: August 19, 2022
Published: September 16, 2022

REFERENCES

Avigdor, A., Goichberg, P., Shivtiel, S., Dar, A., Peled, A., Samira, S., Kollet, O., Hershkoviz, R., Alon, R., Hardan, I., et al. (2004). CD44 and hyaluronic acid cooperate with SDF-1 in the trafficking of human CD34+stem/progenitor cells to bone marrow. Blood *103*, 2981–2989.

Vanden Bempt, M., Demeyer, S., Broux, M., De Bie, J., Bornschein, S., Mentens, N., Vandepoel, R., Geerdens, E., Radaelli, E., Bornhauser, B.C., et al. (2018). Cooperative enhancer activation by TLX1 and STAT5 drives development of NUP214-ABL1/TLX1-positive T cell acute lymphoblastic leukemia. Cancer Cell *34*, 271–285.e7.

Ben-Porath, I., Thomson, M.W., Carey, V.J., Ge, R., Bell, G.W., Regev, A., and Weinberg, R.A. (2008). An embryonic stem cell-like gene expression signature in poorly differentiated aggressive human tumors. Nat. Genet. *40*, 499–507.

Bernstein, B.E., Mikkelsen, T.S., Xie, X., Kamal, M., Huebert, D.J., Cuff, J., Fry, B., Meissner, A., Wernig, M., Plath, K., et al. (2006). A bivalent chromatin structure marks key developmental genes in embryonic stem cells. Cell *125*, 315–326.

de Bock, C.E., Demeyer, S., Degryse, S., Verbeke, D., Sweron, B., Gielen, O., Vandepoel, R., Vicente, C., Vanden Bempt, M., Dagklis, A., et al. (2018). HOXA9 cooperates with activated JAK/STAT signaling to drive leukemia development. Cancer Discov. *8*, 616–631.

Boila, L.D., Chatterjee, S.S., Banerjee, D., and Sengupta, A. (2018). KDM6 and KDM4 histone lysine demethylases emerge as molecular therapeutic targets in human acute myeloid leukemia. Exp. Hematol. *58*, 44–51.e7.

Bonnet, D., and Dick, J.E. (1997). Human acute myeloid leukemia is organized as a hierarchy that originates from a primitive hematopoietic cell. Nat. Med. *3*, 730–737.

Boyd, A.L., Aslostovar, L., Reid, J., Ye, W., Tanasijevic, B., Porras, D.P., Shapovalova, Z., Almakadi, M., Foley, R., Leber, B., et al. (2018). Identification of chemotherapy-induced leukemic-regenerating cells reveals a transient vulnerability of human AML recurrence. Cancer Cell *34*, 483–498.e5.

Buenrostro, J.D., Giresi, P.G., Zaba, L.C., Chang, H.Y., and Greenleaf, W.J. (2013). Transposition of native chromatin for fast and sensitive epigenomic profiling of open chromatin, DNA-binding proteins and nucleosome position. Nat. Methods *10*, 1213–1218.

Burnett, A., Wetzler, M., and Löwenberg, B. (2011). Therapeutic advances in acute myeloid leukemia. J. Clin. Oncol. *29*, 487–494.

Chu, X., Zhong, L., Yu, L., Xiong, L., Li, J., Dan, W., Ye, J., Liu, C., Luo, X., and Liu, B. (2020). GSK-J4 induces cell cycle arrest and apoptosis via ER stress and the synergism between GSK-J4 and decitabine in acute myeloid leukemia KG-1a cells. Cancer Cell Int. *20*, 209.

Cohen, A.A., Geva-Zatorsky, N., Eden, E., Frenkel-Morgenstern, M., Issaeva, I., Sigal, A., Milo, R., Cohen-Saidon, C., Liron, Y., Kam, Z., et al. (2008). Dynamic proteomics of individual cancer cells in response to a drug. Science *322*, 1511–1516.

Costello, R.T., Mallet, F., Gaugler, B., Sainty, D., Arnoulet, C., Gastaut, J.A., and Olive, D. (2000). Human acute myeloid leukemia CD34+/CD38- progenitor cells have decreased sensitivity to chemotherapy and Fas-induced apoptosis, reduced immunogenicity, and impaired dendritic cell transformation capacities. Cancer Res. *60*, 4403–4411.

Cripe, L.D., Uno, H., Paietta, E.M., Litzow, M.R., Ketterling, R.P., Bennett, J.M., Rowe, J.M., Lazarus, H.M., Luger, S., and Tallman, M.S. (2010). Zosuquidar, a novel modulator of P-glycoprotein, does not improve the outcome of older patients with newly diagnosed acute myeloid leukemia: a randomized, placebo-controlled trial of the Eastern Cooperative Oncology Group 3999. Blood *116*, 4077–4085.

Dalerba, P., Kalisky, T., Sahoo, D., Rajendran, P.S., Rothenberg, M.E., Leyrat, A.A., Sim, S., Okamoto, J., Johnston, D.M., Qian, D., et al. (2011). Single-cell dissection of transcriptional heterogeneity in human colon tumors. Nat. Biotechnol. *29*, 1120–1127.

Dalvi, M.P., Wang, L., Zhong, R., Kollipara, R.K., Park, H., Bayo, J., Yenerall, P., Zhou, Y., Timmons, B.C., Rodriguez-Canales, J., et al. (2017). Taxane-platin-resistant lung cancers Co-develop hypersensitivity to JumonjiC demethylase inhibitors. Cell Rep. *19*, 1669–1684.

van Dijk, A.D., Hoff, F.W., Qiu, Y.H., Chandra, J., Jabbour, E., de Bont, E.S.J.M., Horton, T.M., and Kornblau, S.M. (2021). Loss of H3K27 methylation identifies poor outcomes in adult-onset acute leukemia. Clin. Epigenetics *13*, 21.

Ding, L., Ley, T.J., Larson, D.E., Miller, C.A., Koboldt, D.C., Welch, J.S., Ritchey, J.K., Young, M.A., Lamprecht, T., McLellan, M.D., et al. (2012). Clonal evolution in relapsed acute myeloid leukaemia revealed by whole-genome sequencing. Nature *481*, 506–510.

Easwaran, H., Tsai, H.-C., and Baylin, S.B. (2014). Cancer epigenetics: tumor heterogeneity, plasticity of stem-like states, and drug resistance. Mol. Cell *54*, 716–727.

Eppert, K., Takenaka, K., Lechman, E.R., Waldron, L., Nilsson, B., van Galen, P., Metzeler, K.H., Poeppl, A., Ling, V., Beyene, J., et al. (2011). Stem cell gene expression programs influence clinical outcome in human leukemia. Nat. Med. *17*, 1086–1093.

Fang, C.H., Lin, Y.T., Liang, C.M., and Liang, S.M. (2020). A novel c-Kit/phospho-prohibitin axis enhances ovarian cancer stemness and chemoresistance via Notch3-PBX1 and β-catenin-ABCG2 signaling. J. Biomed. Sci. *27*, 42.

Farge, T., saland, E., de Toni, F., Aroua, N., Hosseini, M., Perry, R., Bosc, C., Sugita, M., Stuani, L., Fraisse, M., et al. (2017). Chemotherapy resistant human acute myeloid leukemia cells are not enriched for leukemic stem cells but require oxidative metabolism. Cancer Discov. *7*, 716–735. CD-16-0441.

Feller, N., van der Velden, V.H.J., Brooimans, R.A., Boeckx, N., Preijers, F., Kelder, A., de Greef, I., Westra, G., te Marvelde, J.G., Aerts, P., et al. (2013). Defining consensus leukemia-associated immunophenotypes for detection of minimal residual disease in acute myeloid leukemia in a multicenter setting. Blood Cancer J. *3*, e129.

Gal, H., Amariglio, N., Trakhtenbrot, L., Jacob-Hirsh, J., Margalit, O., Avigdor, A., Nagler, A., Tavor, S., Ein-Dor, L., Lapidot, T., et al. (2006). Gene expression profiles of AML derived stem cells; similarity to hematopoietic stem cells. Leukemia *20*, 2147–2154.

Giustacchini, A., Thongjuea, S., Barkas, N., Woll, P.S., Povinelli, B.J., Booth, C.A.G., Sopp, P., Norfo, R., Rodriguez-Meira, A., Ashley, N., et al. (2017). Single-cell transcriptomics uncovers distinct molecular signatures of stem cells in chronic myeloid leukemia. Nat. Med. *23*, 692–702.

Göllner, S., Oellerich, T., Agrawal-Singh, S., Schenk, T., Klein, H.-U., Rohde, C., Pabst, C., Sauer, T., Lerdrup, M., Tavor, S., et al. (2016). Loss of the histone methyltransferase EZH2 induces resistance to multiple drugs in acute myeloid leukemia. Nat. Med. *23*, 69–78.

Guryanova, O.A., Shank, K., Spitzer, B., Luciani, L., Koche, R.P., Garrett-Bakelman, F.E., Ganzel, C., Durham, B.H., Mohanty, A., Hoermann, G., et al. (2016). DNMT3A mutations promote anthracycline resistance in acute myeloid leukemia via impaired nucleosome remodeling. Nat. Med. *22*, 1488–1495.

Hashizume, R., Andor, N., Ihara, Y., Lerner, R., Gan, H., Chen, X., Fang, D., Huang, X., Tom, M.W., Ngo, V., et al. (2014). Pharmacologic inhibition of histone demethylation as a therapy for pediatric brainstem glioma. Nat. Med. *20*, 1394–1396.

Heinemann, B., Nielsen, J.M., Hudlebusch, H.R., Lees, M.J., Larsen, D.V., Boesen, T., Labelle, M., Gerlach, L.-O., Birk, P., and Helin, K. (2014). Inhibition of demethylases by GSK-J1/J4. Nature *514*, E1–E2.

Hinohara, K., Wu, H.-J., Vigneau, S., McDonald, T.O., Igarashi, K.J., Yamamoto, K.N., Madsen, T., Fassl, A., Egri, S.B., Papanastasiou, M., et al. (2018). KDM5 histone demethylase activity links cellular transcriptomic heterogeneity to therapeutic resistance. Cancer Cell *34*, 939–953.e9.

Ho, T.-C., LaMere, M., Stevens, B.M., Ashton, J.M., Myers, J.R., O'Dwyer, K.M., Liesveld, J.L., Mendler, J.H., Guzman, M., Morrissette, J.D., et al. (2016). Evolution of acute myelogenous leukemia stem cell properties after treatment and progression. Blood *128*, 1671–1678.

Van Der Holt, B., Löwenberg, B., Burnett, A.K., Knauf, W.U., Shepherd, J., Piccaluga, P.P., Ossenkoppele, G.J., Verhoef, G.E.G., Ferrant, A., Crump, M., et al. (2005). The value of the MDR1 reversal agent PSC-833 in addition to daunorubicin and cytarabine in the treatment of elderly patients with previously untreated acute myeloid leukemia (AML), in relation to MDR1 status at diagnosis. Blood *106*, 2646–2654.

Hosen, N., Park, C.Y., Tatsumi, N., Oji, Y., Sugiyama, H., Gramatzki, M., Krensky, A.M., and Weissman, I.L. (2007). CD96 is a leukemic stem cell-specific marker in human acute myeloid

leukemia. Proc. Natl. Acad. Sci. USA *104*, 11008–11013.

Ikawa, T., Masuda, K., Huijskens, M.J.A.J., Satoh, R., Kakugawa, K., Agata, Y., Miyai, T., Germeraad, W.T.V., Katsura, Y., and Kawamoto, H. (2015). Induced developmental arrest of early hematopoietic progenitors leads to the generation of leukocyte stem cells. Stem Cell Rep. *5*, 716–727.

Ishikawa, F., Yoshida, S., Saito, Y., Hijikata, A., Kitamura, H., Tanaka, S., Nakamura, R., Tanaka, T., Tomiyama, H., Saito, N., et al. (2007). Chemotherapy-resistant human AML stem cells home to and engraft within the bone-marrow endosteal region. Nat. Biotechnol. *25*, 1315–1321.

Jin, L., Hope, K.J., Zhai, Q., Smadja-Joffe, F., and Dick, J.E. (2006). Targeting of CD44 eradicates human acute myeloid leukemic stem cells. Nat. Med. *12*, 1167–1174.

Jung, N., Dai, B., Gentles, A.J., Majeti, R., and Feinberg, A.P. (2015). An LSC epigenetic signature is largely mutation independent and implicates the HOXA cluster in AML pathogenesis. Nat. Commun. *6*, 8489.

Kruidenier, L., Chung, C.w., Cheng, Z., Liddle, J., Che, K., Joberty, G., Bantscheff, M., Bountra, C., Bridges, A., Diallo, H., et al. (2012). A selective jumonji H3K27 demethylase inhibitor modulates the proinflammatory macrophage response. Nature *488*, 404–408.

Lee, T.I., Jenner, R.G., Boyer, L.A., Guenther, M.G., Levine, S.S., Kumar, R.M., Chevalier, B., Johnstone, S.E., Cole, M.F., Isono, K.i., et al. (2006). Control of developmental regulators by polycomb in human embryonic stem cells. Cell *125*, 301–313.

Leith, C.P., Kopecky, K.J., Chen, I.M., Eijdems, L., Slovak, M.L., McConnell, T.S., Head, D.R., Weick, J., Grever, M.R., Appelbaum, F.R., and Willman, C.L. (1999). Frequency and clinical significance of the expression of the multidrug resistance proteins MDR1/P-glycoprotein, MRP1, and LRP in acute myeloid leukemia. Blood *94*, 1086–1099.

Li, Y., Zhang, M., Sheng, M., Zhang, P., Chen, Z., Xing, W., Bai, J., Cheng, T., Yang, F.-C., and Zhou, Y. (2018). Therapeutic potential of GSK-J4, a histone demethylase KDM6B/JMJD3 inhibitor, for acute myeloid leukemia. J. Cancer Res. Clin. Oncol. *144*, 1065–1077.

Liau, B.B., Sievers, C., Donohue, L.K., Gillespie, S.M., Flavahan, W.A., Miller, T.E., Venteicher, A.S., Hebert, C.H., Carey, C.D., Rodig, S.J., et al. (2017). Adaptive chromatin remodeling drives glioblastoma stem cell plasticity and drug tolerance. Cell Stem Cell *20*, 233–246.e7.

Libby, E., and Hromas, R. (2010). Dismounting the MDR horse. Blood *116*, 4037–4038.

Löwenberg, B. (2008). Acute myeloid leukemia: the challenge of capturing disease variety. Hematology, 1–11. https://doi.org/10.1182/asheducation-2008.1.1.

Löwenberg, B., Downing, J.R., and Burnett, A. (1999). Acute myeloid leukemia. N. Engl. J. Med. *341*, 1051–1062.

Löwenberg, B., Ossenkoppele, G.J., van Putten, W., Schouten, H.C., Graux, C., Ferrant, A., Sonneveld, P., Maertens, J., Jongen-Lavrencic, M., von Lilienfeld-Toal, M., et al. (2009). High-dose daunorubicin in older patients with acute myeloid leukemia. N. Engl. J. Med. *361*, 1235–1248.

Lu, H., Xie, Y., Tran, L., Lan, J., Yang, Y., Murugan, N.L., Wang, R., Wang, Y.J., and Semenza, G.L. (2020). Chemotherapy-induced S100A10 recruits KDM6A to facilitate OCT4-mediated breast cancer stemness. J. Clin. Invest. *130*, 4607–4623.

Maganti, H.B., Jrade, H., Cafariello, C., Manias Rothberg, J.L., Porter, C.J., Yockell-Lelièvre, J., Battaion, H.L., Khan, S.T., Howard, J.P., Li, Y., et al. (2018). Targeting the MTF2-MDM2 Axis sensitizes refractory acute myeloid leukemia to chemotherapy. Cancer Discov. *8*, 1376–1389.

Mahadevan, D., and List, A.F. (2004). Targeting the multidrug resistance-1 transporter in AML: molecular regulation and therapeutic strategies. Blood *104*, 1940–1951.

Mallaney, C., Ostrander, E.L., Celik, H., Kramer, A.C., Martens, A., Kothari, A., Koh, W.K., Haussler, E., Iwamori, N., Gontarz, P., et al. (2019). Kdm6b regulates context-dependent hematopoietic stem cell self-renewal and leukemogenesis. Leukemia *33*, 2506–2521.

Mathur, R., Sehgal, L., Havranek, O., Köhrer, S., Khashab, T., Jain, N., Burger, J.A., Neelapu, S.S., Davis, R.E., Samaniego, F., et al. (2017). No title. Haematologica *102*, 373–380.

Meacham, C.E., and Morrison, S.J. (2013). Tumour heterogeneity and cancer cell plasticity. Nature *501*, 328–337.

Ng, S.W.K., Mitchell, A., Kennedy, J.A., Chen, W.C., McLeod, J., Ibrahimova, N., Arruda, A., Popescu, A., Gupta, V., Schimmer, A.D., et al. (2016). A 17-gene stemness score for rapid determination of risk in acute leukaemia. Nature *540*, 433–437.

Nooter, K., Sonneveld, P., Oostrum, R., Herweijer, H., Hagenbeek, T., and Valerio, D. (1990). Overexpression of theMDRL gene in blast cells from patients with acute myelocytic leukemia is associated with decreased anthracycline accumulation that can be restored by cyclosporin-A. Int. J. Cancer *45*, 263–268.

Ohtsu, N., Nakatani, Y., Yamashita, D., Ohue, S., Ohnishi, T., and Kondo, T. (2016). Eva1 maintains the stem-like character of glioblastoma-initiating cells by activating the noncanonical NF-κB signaling pathway. Cancer Res. *76*, 171–181.

Ossenkoppele, G., and Schuurhuis, G.J. (2016). MRD in AML: does it already guide therapy decision-making? Hematology. Am. Soc. Hematol. Educ. Program *2016*, 356–365.

Pang, B., Qiao, X., Janssen, L., Velds, A., Groothuis, T., Kerkhoven, R., Nieuwland, M., Ovaa, H., Rottenberg, S., van Tellingen, O., et al. (2013). Drug-induced histone eviction from open chromatin contributes to the chemotherapeutic effects of doxorubicin. Nat. Commun. *4*, 1908.

Patrawala, L., Calhoun, T., Schneider-Broussard, R., Zhou, J., Claypool, K., and Tang, D.G. (2005). Side population is enriched in tumorigenic, stem-like cancer cells, whereas ABCG2+ and ABCG2- cancer cells are similarly tumorigenic. Cancer Res. *65*, 6207–6219.

Pisco, A.O., and Huang, S. (2015). Non-genetic cancer cell plasticity and therapy-induced stemness in tumour relapse: 'What does not kill me strengthens me. Br. J. Cancer *112*, 1725–1732.

Pisco, A.O., Brock, A., Zhou, J., Moor, A., Mojtahedi, M., Jackson, D., and Huang, S. (2013). Non-Darwinian dynamics in therapy-induced cancer drug resistance. Nat. Commun. *4*, 2467.

Pommier, Y., Leo, E., Zhang, H., and Marchand, C. (2010). DNA topoisomerases and their poisoning by anticancer and antibacterial drugs. Chem. Biol. *17*, 421–433.

Qadir, A.S., Stults, A.M., Murmann, A.E., and Peter, M.E. (2020). The mechanism of how CD95/Fas activates the Type I IFN/STAT1 axis, driving cancer stemness in breast cancer. Sci. Rep. *10*, 1310.

Raha, D., Wilson, T.R., Peng, J., Peterson, D., Yue, P., Evangelista, M., Wilson, C., Merchant, M., and Settleman, J. (2014). The cancer stem cell marker aldehyde dehydrogenase is required to maintain a drug-tolerant tumor cell subpopulation. Cancer Res. *74*, 3579–3590.

Rao, J., Xu, D.-R., Zheng, F.-M., Long, Z.-J., Huang, S.-S., Wu, X., Zhou, W.-H., Huang, R.-W., and Liu, Q. (2011). Curcumin reduces expression of Bcl-2, leading to apoptosis in daunorubicin-insensitive CD34+ acute myeloid leukemia cell lines and primary sorted CD34+ acute myeloid leukemia cells. J. Transl. Med. *9*, 71.

van Rhenen, A., Feller, N., Kelder, A., Westra, A.H., Rombouts, E., Zweegman, S., van der Pol, M.A., Waisfisz, Q., Ossenkoppele, G.J., and Schuurhuis, G.J. (2005). High stem cell frequency in acute myeloid leukemia at diagnosis predicts high minimal residual disease and poor survival. Clin. Cancer Res. *11*, 6520–6527.

Roesch, A., Fukunaga-Kalabis, M., Schmidt, E.C., Zabierowski, S.E., Brafford, P.A., Vultur, A., Basu, D., Gimotty, P., Vogt, T., and Herlyn, M. (2010). A temporarily distinct subpopulation of slow-cycling melanoma cells is required for continuous tumor growth. Cell *141*, 583–594.

Röllig, C., and Ehninger, G. (2015). How I treat hyperleukocytosis in acute myeloid leukemia. Blood *125*, 3246–3252.

Sakaki, H., Okada, M., Kuramoto, K., Takeda, H., Watarai, H., Suzuki, S., Seino, S., Seino, M., Ohta, T., Nagase, S., et al. (2015). GSKJ4, A selective jumonji H3K27 demethylase inhibitor, effectively targets ovarian cancer stem cells. Anticancer Res. *35*, 6607–6614.

Sakamoto, K., Imamura, T., Yano, M., Yoshida, H., Fujiki, A., Hirashima, Y., and Hosoi, H. (2014). Sensitivity of MLL-rearranged AML cells to all-trans retinoic acid is associated with the level of H3K4me2 in the RARα promoter region. Blood Cancer J. *4*, e205.

Sato, H., Preisler, H., Day, R., Raza, a, Larson, R., Browman, G., Goldberg, J., Vogler, R., Grunwald, H., and Gottlieb, A. (1990). MDR1 transcript levels as an indication of resistant disease in acute myelogenous leukaemia. Br. J. Haematol. *75*, 340–345.

Scott, M.T., Korfi, K., Saffrey, P., Hopcroft, L.E.M., Kinstrie, R., Pellicano, F., Guenther, C., Gallipoli, P., Cruz, M., Dunn, K., et al. (2016). Epigenetic reprogramming sensitizes CML stem cells to combined EZH2 and tyrosine kinase inhibition. Cancer Discov. *6*, 1248–1257.

Shaffer, B.C., Gillet, J.P., Patel, C., Baer, M.R., Bates, S.E., and Gottesman, M.M. (2012). Drug resistance: still a daunting challenge to the successful treatment of AML. Drug Resist. Updat. *15*, 62–69.

Sharma, S.V., Lee, D.Y., Li, B., Quinlan, M.P., Takahashi, F., Maheswaran, S., McDermott, U., Azizian, N., Zou, L., Fischbach, M.A., et al. (2010). A chromatin-mediated reversible drug-tolerant state in cancer cell subpopulations. Cell *141*, 69–80.

Shimabe, M., Goyama, S., Watanabe-Okochi, N., Yoshimi, A., Ichikawa, M., Imai, Y., and Kurokawa, M. (2009). Pbx1 is a downstream target of Evi-1 in hematopoietic stem/progenitors and leukemic cells. Oncogene *28*, 4364–4374.

Stetson, L.C., Balasubramanian, D., Ribeiro, S.P., Stefan, T., Gupta, K., Xu, X., Fourati, S., Roe, A., Jackson, Z., Schauner, R., et al. (2021). Single cell RNA sequencing of AML initiating cells reveals RNA-based evolution during disease progression. Leukemias *35*, 2799–2812.

Taube, J.H., Sphyris, N., Johnson, K.S., Reisenauer, K.N., Nesbit, T.A., Joseph, R., Vijay, G.V., Sarkar, T.R., Bhangre, N.A., Song, J.J., et al. (2017). The H3K27me3-demethylase KDM6A is suppressed in breast cancer stem-like cells, and enables the resolution of bivalency during the mesenchymal-epithelial transition. Oncotarget *8*, 65548–65565.

Terwijn, M., van Putten, W.L.J., Kelder, A., van der Velden, V.H.J., Brooimans, R.A., Pabst, T., Maertens, J., Boeckx, N., de Greef, G.E., Valk, P.J.M., et al. (2013). High prognostic impact of flow cytometric minimal residual disease detection in acute myeloid leukemia: data from the HOVON/SAKK AML 42A study. J. Clin. Oncol. *31*, 3889–3897.

Terwijn, M., Zeijlemaker, W., Kelder, A., Rutten, A.P., Snel, A.N., Scholten, W.J., Pabst, T., Verhoef, G., Löwenberg, B., Zweegman, S., et al. (2014). Leukemic stem cell frequency: a strong biomarker for clinical outcome in acute myeloid leukemia. PLoS One *9*, e107587.

Vinogradova, M., Gehling, V.S., Gustafson, A., Arora, S., Tindell, C.A., Wilson, C., Williamson, K.E., Guler, G.D., Gangurde, P., Manieri, W., et al. (2016). An inhibitor of KDM5 demethylases reduces survival of drug-tolerant cancer cells. Nat. Chem. Biol. *12*, 531–538.

Walter, R.B., Othus, M., Burnett, A.K., Löwenberg, B., Kantarjian, H.M., Ossenkoppele, G.J., Hills, R.K., Ravandi, F., Pabst, T., Evans, A., et al. (2015). Resistance prediction in AML: analysis of 4601 patients from MRC/NCRI, HOVON/SAKK, SWOG and MD anderson cancer center. Leukemia *29*, 312–320.

Williams, M.S., Amaral, F.M., Simeoni, F., and Somervaille, T.C. (2020). A stress-responsive enhancer induces dynamic drug resistance in acute myeloid leukemia. J. Clin. Invest. *130*, 1217–1232.

Xie, H., Xu, J., Hsu, J.H., Nguyen, M., Fujiwara, Y., Peng, C., and Orkin, S.H. (2014). Cell stem cell article polycomb repressive complex 2 regulates normal hematopoietic stem cell function in a developmental-stage-specific manner. Cell Stem Cell *14*, 68–80.

Xun, J., Wang, D., Shen, L., Gong, J., Gao, R., Du, L., Chang, A., Song, X., Xiang, R., and Tan, X. (2017). JMJD3 suppresses stem cell-like characteristics in breast cancer cells by downregulation of Oct4 independently of its demethylase activity. Oncotarget *8*, 21918–21929.

Yan, N., Xu, L., Wu, X., Zhang, L., Fei, X., Cao, Y., and Zhang, F. (2017). GSKJ4, an H3K27me3 demethylase inhibitor, effectively suppresses the breast cancer stem cells. Exp. Cell Res. *359*, 405–414.

Yang, F., Teves, S.S., Kemp, C.J., and Henikoff, S. (2014). NIH public access. Biochim.Biophys. Acta *1845*, 84–89.

Yu, X., Munoz-Sagredo, L., Streule, K., Muschong, P., Bayer, E., Walter, R.J., Gutjahr, J.C., Greil, R., Concha, M.L., Müller-Tidow, C., et al. (2021). CD44 loss of function sensitizes AML cells to the BCL-2 inhibitor venetoclax by decreasing CXCL12-driven survival cues. Blood *138*, 1067–1080.

STAR★METHODS

KEY RESOURCES TABLE

REAGENT or RESOURCE	SOURCE	IDENTIFIER
Antibodies		
Rabbit monoclonal anti-Histone 3 (clone D1H2)	Cell Signaling Technology	Cat#4499S; RRID: AB_10544537
Rabbit monoclonal anti-H3K4me1 (clone D1A9-XP)	Cell Signaling Technology	Cat#5326; RRID: AB_10695148
Rabbit monoclonal anti-H3K4me2 (clone C64G9)	Cell Signaling Technology	Cat#9725; RRID: AB_10205451
Rabbit monoclonal anti-H3K4me3 (clone C42D8)	Cell Signaling Technology	Cat#9751; RRID: AB_2616028
Rabbit monoclonal anti-H3K27me3 (clone C36B11)	Cell Signaling Technology	Cat#9733; RRID: AB_2616029
Rabbit monoclonal anti-EZH1 (clone D6F1C)	Cell Signaling Technology	Cat#87528
Rabbit monoclonal anti-EZH2 (clone D2C9)	Cell Signaling Technology	Cat#5246; RRID: AB_10694683
Rabbit monoclonal anti-SUZ12 (clone D39F6)	Cell Signaling Technology	Cat#3737; RRID: AB_2196850
Rabbit polyclonal anti-EED	Millipore	Cat#09-774; RRID: AB_1587000
Mouse monoclonal anti-β-actin (clone C4)	Millipore	Cat#MAB1510R; RRID:AB_2223041
Rabbit polyclonal anti-Mouse Immunoglobulins/HRP	Dako/Agilent Technologies	Cat#P0260; RRID:AB_2636929
Goat polyclonal anti-rabbit IgG-HRP	Santa Cruz Biotechology	Cat#sc-2004; RRID:AB_631746
APC mouse anti-human CD44 (clone G44-26)	BD Biosciences	Cat#559942; RRID: AB_398683
APC mouse anti-human CD243 (ABCB1) (clone UIC2)	Thermo Fisher Scientific	Cat#17-2439-42; RRID: AB_10736477
HV500c mouse anti-human CD45 (clone 2D1)	BD Biosciences	Cat#647449
KO mouse anti-human CD45 (clone J.33)	Beckman Coulter	Cat#A96416
PE mouse anti-human CD117 (clone 104D2)	BD Biosciences	Cat#340529; RRID: AB_400044
BV421 mouse anti-human CD34 (clone 581)	BD Biosciences	Cat#562577; RRID: AB_2687922
PC7 mouse anti-human CD34 (clone 581)	Beckman Coulter	Cat#A51077
FITC mouse anti-human CD15 (clone HI98)	BD Biosciences	Cat#560997; RRID: AB_395801
APC-H7 mouse anti-human HLA-DR (clone L243 G46-6)	BD Biosciences	Cat#561358; RRID: AB_10611876
FITC mouse anti-human CD7 (clone M-T701)	BD Biosciences	Cat#555360; RRID: AB_395763
APC mouse anti-human CD7 (clone M-T701)	BD Biosciences	Cat#653311
PE mouse anti-human CD11b (clone D12)	BD Biosciences	Cat#347557
FITC mouse anti-human CD11b (clone Bear1)	Beckman Coulter	Cat#IM0530U
PC7 mouse anti-human CD33 (clone D3HL60.251)	Beckman Coulter	Cat#A54824
APC mouse anti-human CD33 (clone P67.6)	Biolegend	Cat#366605; RRID: AB_256575
APC mouse anti-human CD38 (clone HIT2)	BD Biosciences	Cat#555462; RRID: AB_398599
APC-H7 mouse anti-human CD38 (clone HB-7)	BD Biosciences	Cat#656646
PE mouse anti-human CD22 (clone S-HCL-1)	BD Biosciences	Cat#347577
APC-H7 mouse anti-human CD19 (clone SJ25C1)	BD Biosciences	Cat#641395; RRID: AB_1645728
PE mouse anti-human CD3 (clone OKT3)	BD Biosciences	Cat#566684; RRID: AB_2744380
PerCP rat anti-mouse CD45 (clone 30-F11)	BD Biosciences	Cat#557235; RRID: AB_396609
7-AAD monoclonal antibody	BD Biosciences	Cat#559925
Annexin-V-FITC Conjugate	Tau Technologies	Cat#6592S
Biological samples		
Bone marrow or peripheral blood from AML patients	Amsterdam UMC, location VUmc	N/A
Normal bone marrow from otherwise healthy patients undergoing cardiothoracic surgery	Amsterdam UMC, location VUmc	N/A
Chemicals, peptides, and recombinant proteins		
Gibco roswell park memorial institute-1640	Thermo Fisher Scientific	Cat#21875034

(*Continued on next page*)

Continued

REAGENT or RESOURCE	SOURCE	IDENTIFIER
Iscove's modified dulbecco's medium	Thermo Fisher Scientific	Cat#31980048
CellGro-SCGM medium	Cellgenix	Cat#20802-0500
Penicillin/streptomycin	Gibco Life Technologies	Cat#15140122
DNAse I grade II	Sigma Aldrich	Cat# 10104159001
Magnesium chloride	Sigma Aldrich	Cat#M8266-100G
BIT 9500 serum substitute	StemCell Technology	Cat#09500
Ficoll-paque plus separation	Sigma Aldrich	Cat#GE17-1440-03
Recombinant human FLT3-ligand	Peprotech	Cat#300-19
Recombinant human interleukin 3	Peprotech	Cat#200-03
Recombinant human stem cell factor	Peprotech	Cat#300-07
Recombinant human G-CSF	Miltenyi Biotec	Cat#130-096-346
Bovine serum albumin	Sigma-Aldrich	Cat#A3059-100G
Non-fat dried milk powder	Nutricia	Cat#8712400117654
MTT: 3-(4,5-Dimethyl-2-thiazolyl)-2, 5-diphenyl-2H-tetrazolium bromide	Sigma-Aldrich	Cat#M2128; CAS: 298-93-1
Doxorubicin	Pharmachemie, Teva group	N/A
Daunorubicin	Sanofi	N/A
GSK-J4	Sigma-Aldrich	Cat#SML0701
GSK-J5	Cayman Chemical	Cat#CAY12074
TRIzol reagent	Thermo Fisher Scientific	Cat#15596026
Complete protease inhibitor cocktail	Roche	Cat#11697498001
PhosStop	Roche	Cat#4906845001
Human placental RNAsin	Sphaero Q	Cat#RI01b
Taqman gene expression master mix	Thermo Fisher Scientific	Cat#4369016
Methocult H4354 classic without erythropoietin	StemCell Technologies	Cat#04534
Dharmacon Accell siRNA delivery media	Horizon	Cat#B-005000-500
Retronectin recombinant human fibronectin fragment	Takara Bio Inc	Cat#T100B
Blasticidin S HCl	Thermo Fisher Scientific	Cat#R210-01
Puromycin	InvivoGen	Cat#ant-pr-1
Critical commercial assays		
Bio-rad protein assay	Bio-rad	Cat#5000001
Asherham ECL western blotting detection reagent	Cytiva	Cat#RPN2134
M-MLV reverse transcriptase kit	Invitrogen	Cat#28025013
Flow-count fluorospheres	Beckman Coulter	Cat#7547053
Human CD3 microbeads	Miltenyi Biotec	Cat#130-050-101
TruSeq RNA library prep kit v2	Illumina	Cat#RS-122-2001
TruSeq SBS v3-Kit	Illumina	Cat#FC-401-3002
Magnetic protein G beads	Cell Signaling Technology	Cat#9600
Magnetic protein A + G beads	Magna ChIP	Cat#16-663
Drosophila melanogaster spike-in chromatin	Active Motif	Cat#53083
Nextera XT DNA library preparation kit	Illumina	Cat#FC-131-1024
Agencourt AMPure beads	Beckman Coulter	Cat#15522534
MinElute Reaction Cleanup kit	Qiagen	Cat#28206
Deposited data		
Raw and analyzed data	This paper	GEO: GSE210916

(*Continued on next page*)

Continued

REAGENT or RESOURCE	SOURCE	IDENTIFIER
Experimental models: Cell lines		
K562	AmericanType Culture Collection	Cat#CCL-243; RRID: CVCL_0004
HEK293T	AmericanType Culture Collection	Cat#CRL-3216; RRID: CVCL_0063
Experimental models: Organisms/strains		
Mouse: NOD.Cg-*Prkdc*^{scid} *Il2rg*^{tm1Wjl}*/SzJ (NOD/SCID/IL2r gamma)*	Jackson Laboratory	JAX#005557; RRID: IMSR_JAC:005557
Oligonucleotides		
dNTP set	Roche	11969064001
Primer random p(DN)6	Roche	11034731001
Primer: GUS Forward: 5′-GAAAATATGT GGTTGTTGGAGAGCTCATT-3′	Biolegio BV	N/A
Primer: GUS Reverse: 5′-CCGAGT GAAGATCCCCTTTTTA-3′	Biolegio BV	N/A
GUS probe: 5′-CCAGCACTCTCG TCGGTGACTGTTCA-3′	Biolegio BV	N/A
Primer: PBGD Forward: 5′-GGCAA TGCGGCTGCAA-3′	Biolegio BV	N/A
Primer: PBGD Reverse: 5′-GGGTA CCCACGCGAATCAC-3′	Biolegio BV	N/A
PBGD probe: 5′-CATCTTTGG GCTGTTTTCTTCCGCC-3′	Biolegio BV	N/A
STAT5B (Hs00560026_m1) probe mix	Thermo Fisher Scientific	Cat#4331182
BCL2 (Hs00608023_m1) probe mix	Thermo Fisher Scientific	Cat#4331182
KDM6A (Hs00253500_m1) probe mix	Thermo Fisher Scientific	Cat#4331182
KDM6B (Hs00996325_g1) probe mix	Thermo Fisher Scientific	Cat#4331182
EZH1 (Hs00949463_m1) probe mix	Thermo Fisher Scientific	Cat#4331182
EZH2 (Hs00544830_m1) probe mix	Thermo Fisher Scientific	Cat#4331182
Accell non-targeting control pool siRNAs	Horizon	Cat#D-001910-10-05
Accell KDM6A siRNA SMARTpool	Horizon	Cat#E−014140-00-0005
Accell KDM6B siRNA SMARTpool	Horizon	Cat#E−023013-00-0005
sgRNA KDM6A #1 target sequence: AGGATTCATAGAGAGTGCCT (exon 11)	This paper	N/A
sgRNA KDM6A #2 target sequence: CCTAGCAATTCAGTAACACA (exon 17)	This paper	N/A
sgRNA KDM6B #1 target sequence: AGCAGTCGGAAACCGTTCTT (exon 11)	This paper	N/A
sgRNA KDM6B #2 target sequence: GACAAA AGTACTGTTATCGG (exon 11)	This paper	N/A
Primer: KDM6A exon 11 Forward: 3′-AAGCA GTTCTTCTGAGTTGAC-5′	This paper	N/A
Primer: KDM6A exon 11 Reverse: 3′-ATG TGG CTT TAA AAA ACT GCC-5′	This paper	N/A
Primer: KDM6A exon 17 Forward: 3′-AGG TCA GAG TTC CAC ATT CGG C-5′	This paper	N/A

(*Continued on next page*)

Continued

REAGENT or RESOURCE	SOURCE	IDENTIFIER
Primer: KDM6A exon 17 Reverse: 3′-GTG TGC CTG CTT GTT TCA GGC-5′	This paper	N/A
Primer: KDM6B exon 11 Forward: 5′-AGCAATG CTCCTACCACCTGC-3′ or 5′-CCA GGA AGA GGA GAA GAA GCC-3′	This paper	N/A
Primer: KDM6B exon 11 Reverse: 5′-AAGATC CTCCTCCATCCTCTCGG-3′ or 5′-TAGAGAAC TGAGATGACGAGG-3′	This paper	N/A
Recombinant DNA		
pLenti-Cas9-Blast	This paper	N/A
pCDH-CMV-MCS-EF1alpha-puro	System Biosciences	Cat#CD510B-1
pMDLg/pRRE	Addgene	Cat#12251
pMD2.G	Addgene	Cat#12259
pRSV-Rev	Addgene	Cat#12253
pLCKO	Addgene	Cat#73311
pMSCV-puro	Clontech	Cat#K1062-1
MSCV-JMJD3	Addgene	Cat#21212
MSCV JMJD3 mutant (KDM6B-H1390A)	Addgene	Cat#21214
Software and algorithms		
GraphPad Prism Software (v.8.0)	GraphPad Software Inc.	https://www.graphpad.com/
BD FACSDIVA Software	BD Biosciences	N/A
DAVID (v.8)	LHRI	https://david.ncifcrf.gov/
STRING (v11.5)	STRING Consortium	https://string-db.org/
GSEA (v4.1.0)	Broad Institute Software	https://www.gsea-msigdb.org/gsea/index.jsp

RESOURCE AVAILABILITY

Lead contact

Further information and requests for resources and reagents should be directed to and will be fulfilled by the lead contact, Linda Smit (li.smit@amsterdamumc.nl).

Materials availability

This study did not generate new unique reagents.

Data and code availability

- RNA-seq data is available in NCBI's Gene Expression Omnibus (GEO; http://www.ncbi.nlm.nih.gov/geo) accession number GSE210916.
- This article does not report original code.
- Any additional information required to reanalyze the data reported in this article is available from the lead contact on request.

EXPERIMENTAL MODEL AND SUBJECT DETAILS

Animals

NOD/SCID/IL2r gamma (null) mice (NSG) were purchased from The Jackson Laboratory. All mice were maintained in a specific pathogen-free facility at the Amsterdam Animal Research Center (AARC) of the VU University in accordance with protocols approved by the 'Centrale Commissie Dierproeven' under number 850-HEMA17-02. At the start of the experiments, female and male mice were 6–10 weeks old.

Cell lines, cell culture and isolation of ATCs

K562 cells were purchased from the AmericanType Culture Collection (ATCC) and cultured in Roswell Park Memorial Institute-1640 (RPMI) medium with 10% fetal calf serum (FCS). For making doxorubicin tolerant cells, 5x 96 well plates (Corning) were seeded with 10,000 cells/well. Two days post seeding, treatment with 100 ng/mL doxorubicin was started. After 3 days, part of the cells was passaged to new 96-well plates containing 225 ng/mL doxorubicin. Four weeks later, 21 wells containing viable cells that survived chemotherapy treatment were transferred to new wells in a 96 well plates containing 225 ng/mL doxorubicin. Subsequently, cells from 4 wells could be maintained in culture in the presence of 225 ng/mL doxorubicin.

Primary AML cell cultures

Human AML material was obtained from patients hospitalized at Amsterdam UMC, location VUmc (The Netherlands), at the time of diagnosis and follow up, according to HOVON AML protocols. Normal bone marrow was obtained from otherwise healthy patients undergoing cardiothoracic surgery. Informed consent was obtained from every patient sample used, procedures were approved by the ethical committee of Amsterdam UMC, and all experiments were conducted in accordance with the Declaration of Helsinki.

Mononuclear cells were isolated using Ficoll-Paque PLUS separation and cryopreserved in liquid nitrogen. Samples were thawed in Iscove's Modified Dulbecco's Medium (IMDM) with 20% FCS and incubated with 10 mg/mL DNase I and 10 mM magnesium chloride for 30 min. Samples were cultured in IMDM containing 15% BIT 9500 serum substitute, 50 ng/mL Flt3L, 20 ng/mL IL3, 100 ng/mL human SCF and 20 ng/mL G-CSF in a humidified atmosphere at 37°C and 5% CO2.

METHOD DETAILS

Cell viability assays

K562 cells and primary AML samples were seeded in 96-well plates (Corning) at a density of 10,000–30,000 cells/well and incubated with increasing concentrations of doxorubicin, daunorubicin, GSK-J4 or GSK-J5 for 96 h. 15 μL MTT reagent (3-[4,5-dimethylthiazol-2-yl]-2,5- diphenyltetrazolium bromide) was added and cells were incubated for 4 h (K562) and 6 h (primary AML samples) at 37°C and 5% CO2. Subsequently, MTT crystals were dissolved in 150 μL isopropanol-HCl and absorbance was measured at 540 nm and corrected for background at 720 nm using an Anthos-Elisa-Reader 2001 (Labtec). Values are represented as percentages, using the formula optical density (OD) = (OD treated sample/OD untreated sample) *100.

Immunoblotting

Cell lines and primary AML cells were treated with doxorubicin or GSK-J4 for 48–96 h before analysis. Cells were lysed in 1% NP-40 lysis buffer (50 mM Tris, pH 7.5, 150 mM NaCl, 1% NP40, 5 mM EDTA pH 8.0) containing protease inhibitor cocktail and PhosSTOP. Protein concentrations were determined using a Bio-Rad protein assay. 3OD of cell lysates were boiled in reduced sample buffer for 5 min, proteins were separated by 4–16% precast SDS-PAGE gels (Bio-Rad) and transferred to polyvinylidene fluoride membranes (Millipore) in Tris/glycine/SDS/20% methanol buffer. Membranes were blocked using 2.5% (w/v) non-fat dried milk powder and 2.5% (w/v) BSA in PBS/0.1% Tween (PBS/T) and incubated with first antibodies (1:1000): rabbit anti-Histone 3 (D1H2-XP), rabbit anti-H3K4me1 (D1A9-XP), rabbit anti-H3K4me2 (C64G9), rabbit anti-H3K4me3 (C42D8), rabbit anti-H3K27me3 (C36B11), rabbit anti-EZH1 (D6F1C), rabbit anti-EZH2 (D2C9), rabbit anti-SUZ12 (D39F6), rabbit anti-EED or mouse anti-β-actin (C4, 1:5000). After washing with PBS/T, membranes were incubated with rabbit anti-mouse-IgG-horse radish peroxidase (HRP) (1:1000) or goat anti-rabbit-HRP (1:1000). After washing with PBS/T, membranes were developed with enhanced chemiluminescence and imaged using an UVITEC imaging system (Cleaver Scientific).

RNA isolation and Q-RT-PCR

RNA was isolated using TRIzol according to manufacturer's protocol. Concentration and quality of the RNA was determined with a Nanodrop 1000 (Thermo Fisher Scientific). For cDNA synthesis, 1000 ng of RNA was incubated for 5 min at 65°C, and subsequently incubated with reverse transcriptase buffer, 1 mM DTT, 1 mM dNTPs, 1.89 μg pdN6, 300 U/μlM-MLV reverse transcriptase and 40 U/μl RNasin in nuclease-free water, and incubated for 2 h at 37°C and 10 min at 65°C. Q-RT-PCR reactions were performed in triplicate with 2 μL cDNA [1 μg], 10 μL TaqMan Gene Expression Master Mix, 1 μL 20xTaqman Gene Expression Assay

probe mix and 7 μL nuclease-free water. Expression of housekeeping gene *GUS* or *PBGD* (0.3μM Fw primer, 0.3μM Rv primer and 0.2 μM probe) was used as a control. Q-RT-PCR reactions were performed on an ABI7500 real-time PCR System (Applied Biosystems): 10 min at 95°C followed by 45 cycles at 95°C for 15 s and 60°C for 1 min.

Immunostaining and flow cytometry analysis

Cell lines were incubated with CD44-APC-H7 (G44-26) 1:50, ABCB1 (CD243-APC, UIC2) 1:200, and 7-AAD 1:10 for 15 min and washed with PBS/0.1% human serum albumin (PBS/HSA). After *ex vivo* and *in vivo* treatment, primary AML cells (at diagnosis or MRD) were stained with anti-human CD45-HV500c (2D1) 1:20 or CD45-KO (J.33) 1:20, CD117-PE (104D2), CD34-BV421 (581) 1:20 or CD34-PC7 (581) 1:50, CD15-FITC ((HI98), HLA-DR-APC-H7 (L243 G46-6), CD7-FITC (M-T701) 1:20 or CD7-APC (M-T701) 1:10, CD11b-PE (D12) 1:20 or CD11b-FITC (Bear1) 1:10, CD33-PC7 (D3HL60.251) 1:20 or CD33-APC (P67.6) 1:50, CD38-APC (HIT2) 1:50 or CD38-APC-H7 (HB-7) 1:50, CD22-PE (S-HCL-1) 1:20, CD19-APC-H7 (SJ25C1) 1:20, CD3-PE (OKT3) 1:20, or anti-mouse CD45-PerCP (30-F11) 1:50 for 30 min and washed with PBS/HSA. For detection of apoptosis, cells were labeled with 7-AAD 1:10 for 15–30 min, washed with PBS/HSA, and/or labeled with Annexin V-FITC 1:1000 in binding buffer for 15 min on ice. Flow count fluorospheres were added according to manufacturer's instructions directly before analysis using a FACS-CANTO or FACS-Fortessa flow cytometer (BD Biosciences). Data analysis was performed using FACS Diva software (BD Biosciences).

Liquid culture- and colony forming unit assay

Primary cells were cultured in CellGro-SCGM medium supplemented with 1% penicillin/streptomycin, 50 ng/mL Flt3L, 20 ng/mL IL3 and 100 ng/mL human SCF. After treatment with GSK-J4 for 7 days, 10,000 NBM cells or 50,000 AML cells were transferred to MethoCult without erythropoietin and incubated in a humidified atmosphere at 37°C and 5% CO_2. After 10–14 days, colonies were quantified using an Axiovert 25 bright field microscope (Zeiss).

AML patient-derived xenograft model

Mice were irradiated with 200 cGy one day before injection of T-cell depleted primary AML cells. Primary AML cells were thawed, incubated with anti-CD3 microbeads, and T-cell depleted using MACS columns (Miltenyi Biotec) according to manufacturer's protocol. 1.0–2.2 × 10^6 cells were intravenously injected in the tail vain of the mice. When human CD45 cells were observed in the peripheral blood of the mice, treatment started.

To evaluate the ability of GSK-J4 to reduce leukemic engraftment, mice were intravenously injected with PBS or 10 mg/kg GSK-J4 for 4 times in week 8 (days 1–4) or PBS or 15 mg/kg GSK-J4 for 6 times in week 10 (days 1, 3, 7) and week 13 (days 1, 4, 7). To evaluate if GSK-J4 treatment adds to chemotherapy, mice were intravenously injected with PBS, 15 mg/kg GSK-J4, 1.5 mg/kg doxorubicin, or the combination in week 10 (days 1, 3, 7) and/or week 13 (days 1, 4, 7). Mice were sacrificed when disease features such as ≥20% weight loss were observed or at the endpoint at 16–20 weeks. Bone marrows and spleens were analyzed for presence of human cells using a FACS-Canto flow cytometer (BD Biosciences) and data analysis was performed using FACS Diva software (BD Biosciences).

For secondary transplants of AML-engrafted mice, equal numbers of pooled human myeloid $CD45^+CD33^+$ BM cells derived from first recipients were intravenously injected into the tail vain of irradiated NSG mice. AML engraftment of secondary recipients was assessed as described above.

siRNA knockdown

K562 parental cells and ATC#1–3 were cultured in Accell siRNA delivery media for 24 h at a starting density of 100.000 cells/mL and treated with Accell non-targeting control pool siRNAs or Accell KDM6A or KDM6B siRNA SMARTpool at a final concentration of 1 μM in 100 μL volume per 96-well for 72 h. Viability and gene knockdown was determined with an MTT assay and Q-RT-PCR, respectively.

CRISPR-Cas9 induced knockout of KDM6A and KDM6B

HEK293T cells were transfected with lentiviral constructs (pLenti-Cas9-Blast or pCDH-CMV-MCS-EF1alpha-puro. A total of 12 μg plasmid DNA mix containing lentiviral constructs, 3 μg pMD2G, 5 μg pRRE

and 2.5 μg PRSV-REV were mixed with 150 mM calcium chloride in HEPES-buffered saline and added to HEK293T cells. Medium was harvested after 48–72 h. Retronectin-coated plates were incubated with virus, centrifuged at 3000 rpm for 2 h, and AML cells were added. Transduced cells were selected using 10 μg/mL blasticidin for at least 4 weeks.

To target both the KDM6A and KDM6B genes in Cas9 expressing K562 parental cells and ATC#1–3, designated target sequences were cloned into the sgRNA expressing pLCKO lentiviral backbone. For KDM6A #1 AGGATTCATAGAGAGTGCCT in exon 11 and #2 CCTAGCAATTCAGTAACACA in exon 17, and for KDM6B#1 AGCAGTCGGAAACCGTTCTT in exon 11 and #2 GACAAAAGTACTGTTATCGG in exon 11. Successful cloning in the pLCKO backbone was verified by Sanger sequencing. HEK293 T cells were transfected with lentiviral constructs as described above, and lentivirus was used to transduce Cas9 expressing parental cells and ATC#1–3 (KDM6A gRNA#1 and #2 together, KDM6B gRNA#1 and #2 together, KDM6A and KDM6B combined gRNA#1A and #1B together). Cell were selected by 2 μg/mL puromycin for three days and clones were generated by culturing 0.3 cells per well in 96-well plates. The clones that survived the knockout strategy were counted and the region of KDM6A and/or KDM6B affected by CRISPR-Cas9 was amplified and sequenced using KDM6A exon 11, KDM6A exon 17, and KDM6B exon 11 forward and reverse primers.

Transient transfection to overexpress KDM6B

A total of 5×10^6 K562 cells were transient transfected with control vector (pMSCV-puro), MSCV JMJD3 or MSCV JMJD3 mutant (KDM6B-H1390A), using the Gemini K562 online protocol (BTX Instrument Division, Harvard Apparatus, Inc). In brief, cells were centrifuged and suspended in 1 mL RPMI without FCS, transferred to a pre-chilled 4 mm gap electroporation cuvette and transfected with 12 μg plasmid applying 1 pulse at 250 V for 9 ms. After transfection, cells were cultured in RPMI medium with 10% FCS and selected with 2 μg/mL puromycin for 3 days. Transfected cells were treated with increasing concentrations of doxorubicin for 4 days and viability was determined by MTT assay.

RNA sequencing

Total RNA was extracted with TRIzol according to manufacturer's protocol. Quality of RNA was measured on a 2100 Bioanalyzer (Agilent). Sequencing libraries, each with individual Illumina indexes, were constructed using the TruSeq Stranded mRNA procedure (Sample Prep Kit v2). A mixture of 10 p.m. libraries were pooled equimolar and the resulting DNA was clustered onto a V3 flow cell lane using a c-Bot cluster station and subsequently sequenced in single read fashion for 50bp using a TruSeq SBS v3-Kit and HiSeq2000 Sequencing System (Illumina). Sequence reads were aligned to the human reference genome. The R package DE-Gseq was used to determine differentially expressed genes between purified samples. For interpretation of gene expression data, functional pathway analysis was performed using DAVID (v6.8), protein-protein interaction was performed using String, and gene set enrichment analysis was performed using Broad Institute Software (v4.1.0).

ChIP-sequencing

Briefly, 15×10^6 K562 parental cells and ATCs were washed with PBS and cross-linked with 1% formaldehyde for 10minat room temperature and then quenched by addition of 125 mM glycine. For nuclei isolation, cells were resuspended in 1X RSB buffer (10 mM Tris pH7.4, 10 mM NaCl, 3 mM $MgCl_2$) and left on ice for 10 min to swell. Cells were collected by centrifugation and resuspended in RSBG40 buffer (10 mM Tris pH7.4, 10 mM NaCl, 3 mM $MgCl_2$, 10% glycerol, 0.5% NP40) with 1/10 v/v of 10% detergent (3.3% w/v sodium deoxycholate, 6.6% v/v Tween-40). Nuclei were collected by centrifugation and resuspended in L3B+ buffer (10 mM Tris-Cl pH 8.0, 100 mM NaCl, 1 mM EDTA, 0.5 mM EGTA, 0.1% sodium deoxycholate, 0.5% N-Lauroylsarcosine, 0.2% SDS). Chromatin was fragmented to 200–400 bp using 30 cycles (30 s on, 30 s off, High Setting) using a Bioruptor (Diagenode). Chromatin immunoprecipitation (ChIP) was carried out overnight in the presence of antibodies (H3K27me3; H3K4me3) conjugated to magnetic protein A/G beads (Protein G; Protein A + G). During ChIP, *Drosophila melanogaster* chromatin was introduced or "spiked-in" (50 ng; Spike-in Chromatin) to the chromatin/IP mixture for peak normalization and quantification. Tagmentation (Nextera DNA Sample Preparation Kit) and library preparation was carried out as described (http://www.medical-epigenomics.org/papers/schmidl2015/). DNA was purified using three sided SPRI bead cleanup using 1.0X; 0.65X; 0.9X ratios (Agencourt AMPure Beads) and sequenced on a HiSeq4000 Sequencing System (Illumina). Raw sequencing data were cleaned with fastq-mcf (ea-utils) and mapped to the human reference genome (hg38) using Bowtie2. Quality control was performed with fastqc. The

mapped files were further processed with SAMtools and normalized with deepTools. Peak calling was performed using MACS1.4 and the peaks were further processed with bedtools. To identify the differential peaks, HTSeq-count was used to count the number of reads per peak and the differential analysis was performed with the R-package DESeq2. Custom scripts were utilized to annotate the peaks.

ATAC-sequencing

The Fast ATAC-seq protocol suitable for primary hematopoietic cells was used (Vanden Bempt et al., 2018; de Bock et al., 2018). Per condition, 1 × 10^5 cells were spun down 5 min on 500x*g* at 4°C. Supernatant was carefully removed without disturbing the cell pellet. The cell pellet was resuspended in 50 μL transposase mixture (25 μL 2X TD buffer; 2.5 μL TD enzyme, both from Nextera DNA Library Preparation Kit, Illumina; 0.5 μL 1% digitonin; 22 μL nuclease-free water). Tagmentation reactions were incubated for 30 min at 37°C in a thermal cycler. Tagmented DNA was purified using a MinElute Reaction Cleanup kit. Purified DNA was eluted in 22 μL nuclease-free water. Library preparation and amplification was carried out using the Nextera DNA Sample Preparation Kit, as described previously (Buenrostro et al., 2013). DNA was purified using three sided SPRI bead cleanup using 1.2X; 0.55X; 1.5X ratios (Agencourt AMPure Beads) and sequenced on a HiSeq2000 Sequencing System (Illumina). The ATAC-seq data was analyzed similar to the ChIP-seq data.

Molecular diagnostics and cytogenetic analysis

From isolated mononuclear cells, DNA and/or RNA was studied for the presence of t(9; 22), t(8; 21), t(15; 17), inv16, and mixed-lineage leukemia (MLL) translocations, CEBPα, FLT3-ITD, NPM1, IDH1/2, DNMT3a, c-kit, Jak2, RUNX1, ASXL1, WT1, and tet2 mutations, and EVI1 overexpression by PCR according to standard procedures (www.modhem.nl) recognized by ISO15189. Cytogenetics were determined according to standard techniques and karyotypes were described according to the International System for Human Cytogenetic Nomenclature.

QUANTIFICATION AND STATISTICAL ANALYSIS

Statistical analyses were performed using GraphPad Prism 8.0 software. IC50 values were calculated using non-linear regression curve fitting in GraphPad. Results were reported as mean ± SEM or SD. Statistical significance between 2 measurements was determined using 2-tailed (un)paired Student's t-tests. To compare multiple groups, 1- or 2-way ANOVA with a post-hoc Tukey's or Dunnett's multiple comparison tests were used. Statistical details of experiments can be found in the figures and figure legends; *, $p < 0.05$; **, $p < 0.01$; ***, $p < 0.001$; ****$p < 0.0001$.